Published in final edited form as:
Chem Biol. 2011 June 24; 18(6): 777–793. doi:10.1016/j.chembiol.2011.04.012.

Neuronal store-operated calcium entry pathway as a novel therapeutic target for Huntington's disease treatment

Jun Wu[1,*], **Hsin-Pei Shih**[2,*,#], **Vladimir Vigont**[3,*], **Lori Hrdlicka**[2], **Len Diggins**[2], **Carol Singh**[2], **Matt Mahoney**[2], **Richard Chesworth**[2], **Gideon Shapiro**[2], **Olga Zimina**[3], **Xuesong Chen**[1], **Qingqing Wu**[1], **Lyubov Glushankova**[3], **Michael Ahlijanian**[2,$], **Gerhard Koenig**[2], **Galina N. Mozhayeva**[3], **Elena Kaznacheyeva**[3], and **Ilya Bezprozvanny**[1,§]

[1]Department of Physiology, UT Southwestern Medical Center at Dallas, TX 75390, USA

[2]EnVivo Pharmaceuticals, Watertown, MA 02472, USA

[3]Institute of Cytology Russian Academy of Sciences, St Petersburg 194064, Russia

Abstract

Huntington's disease (HD) is a neurodegenerative disorder caused by a polyglutamine expansion within Huntingtin (Htt) protein. In the phenotypic screen we identified a class of quinazoline-derived compounds which delayed a progression of a motor phenotype in transgenic *Drosophila* HD flies. We found that the storeoperated calcium (Ca^{2+}) entry (SOC) pathway activity is enhanced in neuronal cells expressing mutant Htt and that the identified compounds inhibit SOC pathway in HD neurons. The same compounds exerted neuroprotective effects in glutamate-toxicity assays with YAC128 MSN primary cultures. We demonstrated a key role of TRPC1 channels in supporting SOC pathway in HD neurons. We concluded that the TRPC1-mediated neuronal SOC pathway constitutes a novel target for HD treatment and that the identified compounds represent a novel class of therapeutic agents for treatment of HD and possibly other neurodegenerative disorders.

Keywords

Huntington's disease; Drosophila; nuclear factor-*k*B inhibitor; capacitative calcium entry; store-operated calcium entry; YAC128 transgenic mice; excitotoxicity; TRPC1

Introduction

Huntington's disease (HD) is an inherited autosomal dominant neurodegenerative disorder caused by a polyQ expansion (>36 glutamine repeats) in Huntingtin (Htt) protein (The. et al., 1993). The pathological hallmark of HD is the loss of medium spiny neurons (MSN) in the striatum, which accounts for the major clinical symptoms of the disease. The clinical picture of HD include chorea, psychiatric disturbance, gradual dementia, and death

§Corresponding author: Dr. Ilya Bezprozvanny, tel: (214) 645-6017, fax: (214) 645-6018, Ilya.Bezprozvanny@UTSouthwestern.edu.
*These authors contributed equally to this work
#Present address: Vertex Pharmaceuticals, Inc, 130 Waverly Street, Cambridge, MA 02139
$Present address: Bristol Myers Squibb, 5 Research Parkway, Wallingford, CT 06492

(Vonsattel and DiFiglia, 1998). The exact cause of striatal neuronal loss in HD remains elusive. Diverse pathological paradigms of HD have been proposed such as transcriptional dysregulation, oxidative stress, mitochondrial dysfunction, ubiquitin-proteasome system impairment, and aberrant caspase activation (Cha, 2007; Gil and Rego, 2008; Imarisio et al., 2008; Petrucelli and Dawson, 2004; Roze et al., 2008; Zhang et al., 2006) . Growing evidence has suggested that abnormalities in Ca^{2+} signaling play an important role in pathogenesis of HD (Bezprozvanny, 2009; Tang et al., 2005). Dopamine signalling antagonist tetrabenazine (selective VMAT2 inhibitor) has been recently approved by the Food and Drug Administration for treatment of HD symptoms in the USA (Bezprozvanny, 2009; HSG, 2006). There is no disease-modifying therapy currently available to prevent the onset of HD symptoms or slow the progression of the disease.

The usual approach to drug discovery is based on developing drugs against previously validated targets, but the target-based approach has not been successful in developing HD therapeutics so far. Another approach is based on phenotypic screens in animal models of the disease. The advantage of phenotypic screening strategy is that it facilitates discovery of potential hits without prior assumptions about pathogenic mechanisms and in the context of the biological complexity that *in vitro* and cell-based models cannot easily achieve (Marsh et al., 2009). To identify potential HD therapeutic agents, we established a phenotypic screen by taking an advantage of *Drosophila* transgenic HD model that has been previously described (Al-Ramahi et al., 2006). In our experiments a small molecule quinazoline-derived compound library was screened for compounds that were able to delay progression of a motor phenotype in transgenic flies following induction of human Htt-128Q fragment expression. As a result of the screen we identified a number of hits that alleviated phenotype of transgenic HD flies.

Evaluation of obtained hits revealed that the same compounds have been previously isolated as inhibitors of nuclear factor-κB (NF-κB) pathway activation in immune cells (Tobe et al., 2003b). It has been previously suggested that these compounds do not inhibit NF-κB directly but act by blocking store-operated calcium (Ca^{2+}) entry (SOC) (Choi et al., 2006), a critical step upstream of NF-κB activation in immune cells. An importance of SOC pathway for neuronal physiology was highlighted in recent studies of STIM2 knockout mice (Berna-Erro et al., 2009), genetic studies in *Drosophila* (Hasan and Venkiteswaran, 2010; Venkiteswaran and Hasan, 2009) and in recent functional studies with neuronal cultures (Gruszczynska-Biegala et al., 2011). In our studies we evaluated activity of isolated compounds as SOC inhibitors in HD neurons and validated their neuroprotective effects in experiments with MSN cultures from YAC128 transgenic mice. We discovered that the neuroprotective effects observed in *Drosophila* HD and YAC128 MSN assays were well correlated with ability of these compounds to inhibit activity of NF-κB and SOC pathways. We also discovered that neuronal SOC pathway is significantly upregulated in mutant Huntingtin expressing neurons. Based on these results we concluded that SOC pathway constitute a novel therapeutic target for treatment of HD and possibly other neurodegenerative disorders.

Results

EVP4593 is an NF-κB pathway inhibitor isolated in the phenotypic screen with *Drosophila* HD transgenic model

Photoreceptor-specific expression of the exon 1–4 fragment of a human *huntingtin* gene with 128Q expansion in *Drosophila* has been reported to result in a neurodegenerative phenotype (Al-Ramahi et al., 2006). We discovered that expression of the same Htt-128Q transgene under control of pan-neuronal promoter leads to progressively impaired motor performance of transgenic HD flies with limb tremors and decreased climbing speed. The

motor phenotype developed by transgenic HD flies can be quantified by dropping the flies to the bottom of the tube and measuring the speed of upward climbing for individual flies. On average the speed of upward climbing was reduced from 12 mm/sec immediately after transgene expression to 5 mm/sec 10 days after transgene expression (Fig 1A, blue line). The climbing speed of control flies expressing LacZ transgene remained constant at 13 mm/sec in the same time period (Fig 1A, red line). To validate this experimental system, we reconfirmed efficacy of several pharmacological compounds published in the previous studies with *Drosophila* HD models, such as histone deacetylase inhibitor inhibitors TSA (Fig 1A, green line) and SAHA (data not shown) and rapamycin (data not shown) (Ravikumar et al., 2004; Steffan et al., 2001). Thus, we concluded that the reproducible, progressive and quantifiable motor deficit observed in transgenic HD flies (Fig 1A) provides an opportunity for screening for novel potential HD therapeutic agents.

In search for such agents we screened a quinazoline-derived small molecule library composed of 521 compounds using the climbing assay as readout and identified several initial hits. The initial hits were used in a structure similarity search and a secondary focused library of additional 72 quinazoline-derived compounds was generated and screened. As a result of the secondary focused library screening we discovered EVP4593 as a potent hit. This compound significantly slowed the progressive decline in the climbing speed of the HD flies (Fig 1A, yellow line). The efficacy of EVP4593 at 400 μM in the climbing assay was superior to the efficacy of TSA at 250 μM (Fig 1A), which was used as a positive control in our experiments (Steffan et al., 2001). The efficacy of TSA at 400 μM could not be tested because of toxicity observed at TSA concentrations above 250 μM (data not shown). To quantify the effects of EVP4593, we measured an average improvement in the climbing speed when compared to HD transgenic flies feed with 1% DMSO. To calculate a magnitude of the observed effects, the difference in the average climbing speed of HD flies resulting from EVP4593 feeding was normalized to the standard deviation in the climbing speed of the entire DMSO-treated group. When the data collected during days 8–10 after transgene induction were averaged, we determined that feeding the flies with 400 μM of EVP4593 resulted in an average effect size of 3.0 ($p < 0.003$) (Fig 1B). The efficacy of EVP4593 was dose-dependent in the range between 100 μM and 400 μM in the fly food (Fig 1B). The EVP4593 had no significant effect on climbing performance of HD flies at 50 μM (Fig 1B). The EVP4593 had no toxic effects on *Drosophila* in the range of concentrations tested in our assays (50 – 400 μM).

EVP4593 is a derivative of 6-aminoquinazoline class (Fig 1C) that has been previously isolated as an inhibitor of PMA/PHA-induced NF-κB pathway activation in Jurkat cells (Tobe et al., 2003b). To determine if the beneficial effects observed in the climbing assay with transgenic HD flies (Fig 1A) are related to inhibition of NF-κB signaling, we selected 7 structural analogs of EVP4593 from the same chemical class (Fig 1C). The efficacy of each of these compounds was evaluated in the climbing assay with HD flies and in PMA/PHA-induced NF-κB assay with human Jurkat cells. The effect size in the climbing assay was measured in the presence of 200 μM of each tested compound in the fly food at days 8–10 after Htt-128Q transgene induction. The inhibition of NF-κB activation was evaluated at 1 μM of each compound. We found that EVP4593, EVP14782, and EVP14756 demonstrated significant potency in climbing assay with effect sizes in the range 2–4 ($p < 0.003$) (Fig 1D). In contrast, EVP14809, EVP14810, EVP14812, and EVP14808 compounds were inactive in the climbing assay (Fig 1D). When evaluated in NF-κB assay, compounds EVP4593, EVP14782, and EVP14756 were also most potent with 50–60% inhibition (Fig 1D). Compounds EVP14809 and EVP14810 were less potent with 20% inhibition and compounds EVP14812, and EVP14808 were unable to inhibit NF-κB activation (Fig 1D).

To get more insight into mechanism of action of these compounds, we evaluated dose-dependence of NF-κB pathway inhibition by these compounds. We discovered that EVP4593, EVP14782, and EVP14756 acted as high affinity partial antagonists of NF-κB pathway activation. These 3 compounds inhibited 50–60% of NF-κB activity with apparent affinities in the nanomolar range (Supplementary Fig 1 and Table 1). Compounds EVP14809 and EVP14810 also acted as partial antagonists of NF-κB activation but with affinities in the micromolar range (Supplementary Fig 1 and Table 1). The compounds EVP14812 and EVP14808 were not able to inhibit NF-κB activation (Supplementary Fig 1 and Table 1). Our analysis revealed excellent correlation between ability of compounds in this chemical series to inhibit PMA/PHA-induced NF-κB activation in human Jurkat cells and to alleviate motor symptoms developed by transgenic HD flies (Fig 1D and Table 1). This correlation was further confirmed by testing 30 more additional analogs from the same chemical class with various potencies of NF-κB inhibition (data not shown).

To determine if direct inhibition of NF-κB is responsible for beneficial effects observed in the climbing assay, we evaluated structurally unrelated compound BMS-345541 (Fig 1C). BMS-345541 is a potent IκB kinase (IKK) inhibitor (Burke et al., 2003), which fully and with high affinity suppressed PMA/PHA-induced NF-κB activation in Jurkat cells in our experiments (Fig 1D and Supplementary Fig 1). However, BMS-345541 at 400 μM was inactive when tested in the climbing assay with transgenic HD flies (Fig 1D). Similarly negative results were obtained in experiments with several additional IKK inhibitors tested in the climbing assay with transgenic HD flies (data not shown). In contrast, EVP4593 was not active when tested in the IKK kinase assay (data not shown). These data suggested that direct inhibition of NF-κB may not be responsible for the beneficial effects observed with EVP4593, EVP14782, and EVP14756 compounds in the climbing assays.

The library of quinazoline class of compounds was chosen initially for our screen as this scaffold often leads to kinase inhibitors, and kinases are considered attractive and tractable drug targets. However, when EVP4593 compound was evaluated at 10 μM concentration in commercial kinase inhibition assays using screening platforms from MDS Pharma Services, Ambit Biosciences, and Millipore we could not detect significant kinase inhibitory activity for this compound (data not shown). All these results suggested that EVP4593 and its active analogs EVP14782 and EVP14756 are likely to inhibit NF-κB activation indirectly. This conclusion is consistent with the partial antagonism displayed by these compounds when tested in PMA/PHA-induced NF-κB activation assay (Supplementary Fig 1), in contrast to the full antagonism displayed in the same assay by BMS-345541 (Supplementary Fig 1). PMA/PHA-induced NF-κB activation depends on activation of protein kinase C (PKC) and Ca^{2+} influx. We determined that EVP4593 does not inhibit PKC in *in vitro* kinase assays (data not shown). Thus, we hypothesized that EVP4593 may act by inhibiting storeoperated Ca^{2+} entry (SOC), a critical upstream step of NF-κB activation in Jurkat cells. Indeed, it has been previously reported that EVP4593 can inhibit SOC in experiments with SH-5Y5 cells (Choi et al., 2006). To test this possibility, we evaluated structurally distinct 2-APB compound (Fig 1C) that is known to act as low affinity SOC inhibitor in some cells (Bootman et al., 2002; Ma et al., 2003). We discovered that when added to fly food at 400 μM, 2-APB also demonstrated significant benefit in the climbing assay (Fig 1D). Interestingly, at 1 μM concentration 2-APB did not inhibit NF-kB activation (Fig 1D), indicating that SOC pathway in Jurkat cells is not efficiently blocked by 2-APB. Based on these results we proposed that EVP4593 and its active analogs EVP14782 and EVP14756 might exert beneficial effect by inhibiting SOC Ca^{2+} entry pathway in neurons of HD flies. To test this hypothesis we set out to determine if EVP4593 and its active analogs act by inhibiting SOC pathway in neuronal cells.

EVP4593 and its active analogs inhibit store-operated Ca^{2+} entry in HD striatal neurons

In our studies we focused on medium spiny striatal neurons (MSN), the main locus of pathology in HD. In the first series of experiments we evaluated the size of SOC in wild type (WT) MSN and YAC128 MSN. The WT and YAC128 MSN were incubated in Ca^{2+}-free media in the presence of 1 μM of SERCA pump inhibitor Thapsigargin (Tg) for 5 min to cause complete depletion of intracellular Ca^{2+} stores. Following complete store depletion the neurons were transferred to the extracellular media containing 2 mM Ca^{2+} and the amplitude of initial cytosolic Ca^{2+} influx following Ca^{2+}-readdition was determined by Fura-2 imaging. In these experiments we observed that the amplitude of SOC Ca^{2+} entry was significantly higher in YAC128 MSN (Fig 2B) than in WT MSN (Fig 2A). On average, the amplitude of SOC Ca^{2+} entry was 0.21 ± 0.02 (n = 38) in WT MSN and 0.30 ± 0.02 (n = 29) in YAC128 MSN ($p < 0.05$) (Fig 2E). We also found the thapsigargin-induced Ca^{2+} release from the ER was reduced in YAC128 MSN when compared with WT (Fig 2A and 2B). Most likely this is due to increased sensitivity of $InsP_3R1$ to activation by $InsP_3$ caused by the presence of the mutant Htt (Tang et al., 2003), which causes increased ER Ca^{2+} leakage at the steady-state conditions. Addition of 300 nM of EVP4593 resulted in strong attenuation of SOC Ca^{2+} influx in YAC128 MSN neurons (Fig 2D). On average the amplitude of SOC Ca^{2+} entry in YAC128 MSN was reduced from 0.30 ± 0.02 (n = 29) in the presence of DMSO control to 0.11 ± 0.02 (n = 54) in the presence of 300 nM of EVP4593 ($p < 0.001$) (Fig 2E). Similar suppression of SOC Ca^{2+} entry was also observed in the presence of 300 nM EVP14756 (Fig 2E). In contrast, inactive analog EVP14808 had no effect on the amplitude of SOC Ca^{2+} entry in YAC128 MSN cells when tested in the same concentration (Fig 2E). Interestingly, SOC pathway in WT neurons was much less sensitive to inhibition by EVP4593. Addition of 300 nM EVP4593 did not inhibit Ca^{2+} increase in WT neurons (Fig 2C) and had no significant effect on the amplitude of SOC-mediated Ca^{2+} elevation in WT neurons (Fig 2E).

To quantitatively compare ability of EVP4593 and its analogs to inhibit SOC pathway in YAC128 MSN, we performed a series of measurements using Mn^{2+}-induced Fura-2 quenching method (Dadsetan et al., 2008; Yang et al., 2005). In our experiments YAC128 MSN were loaded with Fura-2 and incubated in Ca^{2+}-free media in the presence of 30 μM of SERCA pump inhibitor CPA for 10 min to completely deplete Ca^{2+} stores and to activate SOC pathway. Following addition of 150 μM Mn^{2+} to the extracellular solution, Fura-2 quenching was initiated and initial slope of the F_{360} decline was measured (Fig 3A, section a). Five minutes later 1‰ DMSO control or test compounds in 300 nM concentration were added and the rate of Fura-2 quenching was measured again (Fig 3A, section b). The effect of test compounds on SOC activity was estimated by comparing the slope of Fura-2 Mn^{2+} quenching before (section a) and after (section b) addition of the compounds for each cell. In these experiments we found that an addition of DMSO had no effect on the rate of Fura-2 Mn^{2+} quenching (Fig 3A). In contrast, addition of EVP4593 resulted in significant reduction in the rate of Fura-2 Mn^{2+} quenching (Fig 3B). The inactive analog EVP14808 had no significant effect on the Fura-2 Mn^{2+} quenching rate (Fig 3C). To compare results obtained in different experiments, we calculated the ratio of the Fura-2 Mn^{2+} quenching rates observed after (phase b) and before (phase a) addition of the test compounds to each cell. From this analysis we determined that EVP4593, EVP14756 and EVP14782 compounds inhibited SOC pathway activity by approximately 40% when tested at 300 nM (Fig 3D and Table 1). In contrast, inactive analogs EVP14808 and EVP14810 had no significant effect on SOC activity (Fig 3D and Table 1) and EVP14812 appeared to increase the rate of Fura-2 Mn^{2+} quenching (Figure 3D and Table 1). The EVP14809 caused interference with the Mn^{2+} quenching assay and the potency of this compound could not be evaluated by this approach.

EVP4593 inhibits TRPC1-supported SOC Ca^{2+} currents in neuronal cells

To further evaluate an ability of EVP4593 to act as SOC inhibitors we performed a series of electrophysiological experiments. In initial experiments we attempted whole cell recordings of SOC currents in primary mouse MSN cultures. We were able to record thapsigargin-activated Ba^{2+} currents in mouse MSN cultures at the magnitude of 1.0 ± 0.2 (n = 10) pA/pF (data not shown). However, these experiments were technically difficult and it was challenging to obtain stable SOC recordings in MSN primary cultures. Thus, for electrophysiological analysis we selected SK-N-SH human neuroblastoma cells transiently transfected with human Htt-15Q or Htt-138Q expression constructs. The Htt expression constructs were contransfected with EGFP plasmid and transfected cells were identified by GFP fluorescence. In whole cell recordings of Isoc activity we used 10 mM Ba^{2+} as a charge carrier as we previously described for A431 cells (Gusev et al., 2003). Under these conditions, passive store depletion following addition of 1 μM thapsigargin (Tg) induced inward cation currents that reached the maximum within 3 min after addition of Tg (Fig 4A). In these experiments we found that amplitude of Isoc inward currents in nontransfected cells and in the cells transfected with Htt-15Q cells was practically indistinguishable (Fig 4A). At −80 mV holding potential the amplitude of maximal Isoc currents in both groups of cells was equal to 0.45 pA/pF (Figs 4A, 4B, 4C). In contrast, Tg-induced Isoc currents in Htt-138Q cells were much larger (Fig 4A), with maximal currents reaching 2.3 pA/pF at −80 mV (Fig 4A, 4B, 4C). On average, the amplitude of Isoc currents in SK-N-SH cells transfected with Htt-138Q plasmid was 5-times larger than in non-transfected cells or in the cells transfected with Htt-15Q plasmid (Fig 4C). The increased Isoc activity in electrophysiological experiments with neuronal cells transfected with Htt-138Q plasmid is consistent with increased SOC activity that we observed in Ca^{2+} imaging experiments with YAC128 MSNs (Fig 2).

To investigate the ability of EVP4593 to inhibit Isoc currents in SK-N-SH cells transfected with Htt-138Q, we applied 300 nM EVP4593 to the cells after Tg-induced Isoc current was fully activated. We found that addition of EVP4593 resulted in immediate block of Isoc currents in these cells (Fig 4D). Following washout of EVP4593 the amplitude of the Isoc current was partially recovered (Fig 4D), indicating that the inhibition was reversible. In contrast, addition of 300 nM EVP14808 had no effect on Isoc current in Htt-138Q transfected cells, similar to addition of DMSO carrier solution alone (Fig 4D). Addition of 300 nM EVP4593 resulted in approximately 2.5-fold reduction in the magnitude of Isoc currents recorded at −80 mV holding potential in Htt-138Q–transfected cells (Figs 4D, 4E, 4F). In contrast, addition of the same concentration of EVP14808 had no significant effect on Isoc currents in in Htt-138Q-transfected cells (Figs 4D, 4E, 4F). The small Isoc current in non-transfected SK-N-SH cells was sensitive to EVP4593 (Fig 4D), but to a far lesser extent than Isoc current in Htt-138Q-transfected cells (Figs 4D, 4E, 4F). This conclusion is consistent with results obtained in Ca^{2+} imaging experiments with WT and YAC128 MSN (Fig 2).

The molecular composition of neuronal SOC pathway is poorly understood, with potential components including members of mammalian Trp family and Orai1 channels (Berna-Erro et al., 2009; Gruszczynska-Biegala et al., 2011; Hasan and Venkiteswaran, 2010; Putney, 2003; Venkiteswaran and Hasan, 2009). Our electrophysiological measurements indicate that the channels upregulated in SK-N-SH cells in response to Htt-138Q transfection are relatively non-selective (Fig 4B), consistent with the known properties of mammalian TRPC channels (Montell, 2005). It has been recently demonstrated that together with Orai channels TRPC channels play an important role in supporting SOC in Jurkat cells (Wenning et al., 2011), and it is possible that EVP4593 inhibited TRPC-supported currents in our NF-kB activation experiments (Fig 1D). TRPC1 channels are expressed in the nervous system (Riccio et al., 2002) and we reasoned that TRPC1 subunits may play a role in supporting

Isoc currents upregulated in response to Htt-138Q expression. To test this hypothesis, we cotransfected SK-N-SH cells with Htt-138Q plasmid and siRNA plasmid against human TRPC1 subunit. Off-target control siRNA was used as a negative control in these experiments. Expression of endogenous TRPC1 in SK-N-SH cells and the efficiency of siRNA-mediated TRPC1 knockdown in transfected cells were confirmed by Western blotting of cellular lysates (Supplementary Fig 2). In these experiments we found that RNAi-mediated knockdown of TRPC1 significantly reduced Tg-induced Isoc currents in Htt-138Q-transfected cells (Fig 5A). At −80 mV holding potential the amplitude of Isoc currents in these cells was equal to 0.8 pA/pF, comparable to the amplitude of Isoc currents in non-transfected cells (Fig 5A, 5C, 5D). On average, co-transfection of Htt-138Q with TRPC1 RNAi plasmid reduced amplitude of Isoc currents by 70% (Fig 5D). The effect of TRPC1 RNAi was specific, as co-transfection of Htt-138Q with control RNAi had no effect on the amplitude of Isoc currents (Figs 5A, 5C, 5D). In additional experiments we demonstrated that knockdown of TRPC1 by siRNA occluded effects of EVP4593 on Isoc currents in Htt138-transfected cells (Figs 5B, 5C, 5D). These experiments pointed to TRPC1 as one of the subunits of Isoc channels activated in response to Htt- 138Q expression in SK-N-SH cells and inhibited by EVP4593. In additional experiments we demonstrated that RNAi-mediated knockdown of TRPC1 subunit in primary mouse MSN cultures causes significant reduction in the amplitude of thapsigargin-evoked SOC currents (data not shown).

To test the hypothesis that EVP4593 blocks TRPC1-supported channels, we transfected SK-N-SH cells with a mouse TRPC1 expression plasmid. Consistent with the known role of TRPC1 (Clapham et al., 2001), Isoc currents were significantly enhanced in TRPC1-transfected SK-N-SH cells, similar in size to Isoc currents in Htt-138Q-transfected cells (Fig 5A). However, the properties of Isoc currents in TRPC1-transfected cells were different from the properties of Isoc currents in Htt-138Q-transfected cells. The shape of the current-voltage relationship in TRPC1-transfected cells was different, with much larger outward current than in Htt138Q-transfected cells (Fig 5C). Even more strikingly, currents resulting from TRPC1 overexpression were not sensitive to inhibition by EVP4593 (Fig 5B, 5D). From these experiments we concluded that EVP4593 does not target TRPC1 homomeric channels but rather targets heteromeric channels containing TRPC1 as one of the subunits. Western blotting experiments also indicated that the levels of TRPC1 expression remain constant in Htt-138Q-transfected SK-N-SH cells (Supplementary Fig 2). Future experiments will be required to identify the subunit of SOC channels that is upregulated in Htt-138Q-transfected cells and forms heteromeric channels with TRPC1.

EVP4593 and its active analogs protect YAC128 MSN from glutamate toxicity

Do EVP4593 and its analogs exert neuroprotective effects in mammalian model of HD? To answer this question we evaluated activity of EVP4593 and its analogs in glutamate toxicity experiments with primary MSN cultures from YAC128 mice. In the previous studies we described that YAC128 MSN are significantly more susceptible to glutamate-induced apoptosis than WT MSN cultures (Tang et al., 2005). The difference between glutamate-induced apoptosis of YAC128 and WT MSN is significant and consistent, providing a quantitative basis for the *in vitro* HD assay. In the previous studies we took an advantage of this experimental system to evaluate potential neuroprotective effects of a number of clinically relevant compounds (Wu et al., 2009; Wu et al., 2008; Wu et al., 2006). As in previous studies we determined that in the absence of glutamate, approximately 5–15% of neurons were apoptotic in both wild-type (WT) and YAC128 MSN cultures (Fig 6 and Table 2). After addition of 250 μM glutamate, the fraction of apoptotic WT MSN was increased to 30–45% and the fraction of apoptotic YAC128 MSN was increased to 65–80% (Fig 6 and Table 2). The potential neuroprotective effects of EVP4593 and its analogs in our

experiments were evaluated at 30 nM, 300 nM and 3 μM concentrations. In all experiments compounds were added to MSN cultures 30 min prior to addition of glutamate. We found that EVP4593 significantly protected YAC128 MSN from glutamate toxicity at 30 nM and 300 nM concentrations (Fig 6A, 6B and Table 2). EVP14756 was equally potent, with significant protective effects at 30 nM and 300 nM concentrations (Table 2). EVP14782 was not effective at 30 nM but was protective at 300 nM concentration (Table 2). EVP4593, EVP14756 and EVP14782 became cytotoxic when tested in 3 μM concentrations (Table 2). The neurons detached in experiments with 3 μM of EVP4593 and EVP14782 and data could not be collected, while for EVP14756 the toxicity compromised its neuroprotective effect when tested at 3 μM concentration (Table 2). EVP14809 was not effective at 30 nM and 300 nM concentrations, but demonstrated significant neuroprotective effects at 3 μM (Fig 6D and Table 2). EVP14808, EVP14810, and EVP14812 were inactive at any concentrations that were tested (Fig 6C and Table 2). From these results we concluded that when tested in YAC128 MSN excitotoxicity model, EVP4593, EVP14756 and EVP14782 exhibited neuroprotective effects in nanomolar concentrations, EVP14809 was active in micromolar concentration, and EVP14808, EVP14810, and EVP14812 were inactive (Table 1).

Our electrophysiological data suggested that EVP4593 inhibits TRPC1-supported SOC currents and that TRPC1-supported SOC currents are upregulated in response to mutant Htt^{exp} expression (Fig 5). To confirm that neuroprotective effects of EVP compounds are indeed due to inhibition of TRPC1-supported SOC currents, we evaluated neuroprotective effects of TRPC1 RNAi knockdown in YAC128 MSN cultures. In these experiments expression of mouse TRPC1 was suppressed by application of Dicer-mediated approach. The mixture of siRNA (25–27nt in size) targeting mouse TRPC1 was generated as described in Methods and transfected into WT and YAC128 MSN at DIV2 together with non-targeting siRNA. In parallel experiments the cells were treated with transfection reagent (PEI) alone or together with non-targeting siRNA (Ctrl siRNA). In the absence of glutamate, approximately 10–25% of neurons were apoptotic in both wild type (WT) and YAC128 MSN cultures (Fig 6E, 6F, Table 2) in these experiments. The fractions of apoptotic WT and YAC128 MSN treated with non-targeting siRNA increased slightly as a result of transfection procedure (Fig 6E, Table 2), but they were not significantly different from those of WT and YAC128 MSN treated with the transfection reagent alone (Fig 6E, Table 2). After addition of 250 μM glutamate, the fraction of apoptotic WT MSN in transfection reagent control was increased to 30–40% and the fraction of apoptotic YAC128 MSN in transfection reagent control was increased to around 65% (Fig 6E, 6F, Table 2). The results obtained in cells with non-targeting siRNA were identical to results in cells exposed to transfection reagent alone (Fig 6E, Table 2). In contrast, YAC128 MSN treated with TRPC1 siRNA were significantly protected from glutamate-induced apoptosis when compared to transfection reagent control (Fig 6F, Table 2). The fraction of apoptotic WT MSN treated with TRPC1 siRNA was also slightly decreased, but effect was not significant when compared to transfection reagent control (Fig 6F, Table 2). From these experiments we concluded that RNAi-mediated knockdown of TRPC1 subunit protects YAC128 MSN neurons from glutamate-induced apoptosis.

Discussion

In this study we utilized a phenotypic drug screening platform based on a *Drosophila* transgenic HD model to search for potential HD therapeutics. *Drosophila* has been widely used to model HD and other polyglutamine expansion disorders, revealing several conserved cellular pathways important for pathogenesis (Marsh et al., 2009). In several previous studies pharmacological agents alleviated phenotypes developed by *Drosophila* HD models (Desai et al., 2006; Ravikumar et al., 2004; Steffan et al., 2001). The *Drosophila* HD model used in our study expressed first 4 exons of human Huntingtin with 128Q expansion under

control of an inducible promoter (Al-Ramahi et al., 2006). Following induction of Htt-128Q transgene expression in the nervous system, the HD flies developed progressive motor phenotype that can be quantified by using automated climbing assay (Fig 1A). By taking advantage of this reproducible phenotype, we developed a medium-throughput screening platform for potential HD therapeutics.

We used the developed screening platform to screen a library of quinazoline-derived compounds and after secondary round of screening identified a compound EVP4593 as a potent hit (Figs 1A and 1B). The same compound has been previously isolated as an inhibitor of PMA/PHA-induced NF-κB pathway activation in Jurkat cells (Tobe et al., 2003b). In our studies we compared a relative efficacy of EVP4593 and its six structure-related analogs (Fig 1C) in *Drosophila* HD climbing assay and PMA/PHA-induced NF-κB activation assay in Jurkat cells. We observed an excellent correlation between relative potencies demonstrated by all 7 compounds in these assays (Fig 1D and Table 1). Several previous studies suggested that NF-κB pathway might play a direct role in HD pathogenesis. Inhibition of NF-κB activity decreased the striatal lesion in acute excitotoxicity model (Nakai et al., 2000; Qin et al., 2001; Qin et al., 1998). NF-κB activation has been observed in PC12 cells transfected with mutant Huntingtin construct, in R6/2 transgenic HD mice and in HD knock-in mice (Khoshnan et al., 2004; Sugars et al., 2004). The mutant huntingtin has been shown to bind IKK, enhancing IKK activity (Khoshnan et al., 2004). The Htt^{exp}-mediated cell death in HEK-293 cells and striatal slices can be rescued by blocking IKK activity (Khoshnan et al., 2004). Recent studies revealed that IKK can phosphorylate Htt directly and affect its turnover rate (Thompson et al., 2009). All these results suggest that inhibition of NF-κB pathway may provide a potential approach for neuroprotection in HD (Chu et al., 2007).

However further examination of isolated compounds indicated that the inhibition of NF-κB pathway is not likely to be directly responsible for the beneficial effects observed in experiments with transgenic HD flies. Structurally unrelated potent IKK and NF-κB inhibitor BMS-345541 was not effective in the climbing assay with HD flies (Fig 1D). Similarly negative results were obtained in experiments with several additional IKK inhibitors that were tested (data not shown). In contrast to the fully potent inhibitor BMS-345541, EVP4593 and its active analogs acted as partial antagonists of NF-κB pathway (Supplementary Fig 1), consistent with indirect mode of action of these compounds. Moreover, EVP4593 failed to block IKK or PKC directly or exhibit any kinase inhibitory activity in a variety of screening platforms (data not shown). Based on this analysis we hypothesized that EVP4593 may act by inhibiting SOC, which is critical for PMA/PHA-induced NF-κB activation in Jurkat cells. Indeed, it has been previously reported that EVP4593 can inhibit SOC in experiments with SH-5Y5 cells (Choi et al., 2006). In a series of Ca^{2+} imaging and electrophysiological experiments we demonstrated that SOC pathway is upregulated in primary MSN neurons from YAC128 transgenic HD mice (Fig 2) and in SK-N-SH human neuroblastoma cells transfected with Htt-138Q expression plasmid (Fig 4). The up-regulation of SOC pathway was specifically induced by Htt^{exp} and did not occur in SK-N-SH cells transfected with Htt-15Q plasmid (Fig 4). Previous studies demonstrated that the mutant Htt^{exp} affects Ca^{2+} signaling in MSN by increasing the sensitivity of $InsP_3R1$ to $InsP_3$ (Tang et al., 2003), by potentiating function of NR2B–containing NMDAR (Chen et al., 1999; Fan et al., 2007; Milnerwood and Raymond, 2007; Sun et al., 2001; Zeron et al., 2002; Zhang et al., 2008), and by destabilizing mitochondrial Ca^{2+} handling (Choo et al., 2004; Panov et al., 2002). The increase in SOC pathway activity observed in our experiments (Figs 2 and 4) may be a direct result of Htt^{exp} expression or may correspond to a compensatory response of the cells to destabilized Ca^{2+} signaling. Future studies will be required to address this issue.

Consistent with the previous results (Choi et al., 2006), we demonstrated that EVP4593 effectively inhibited SOC pathway in YAC128 MSN (Figs 2 and 3) and in SK-N-SH cells transfected with Htt-138Q (Fig 4). The inactive analog EVP14808 failed to inhibit SOC pathway in either experimental system (Figs 2–4). Interestingly, EVP4593 was much less potent in inhibiting SOC in WT MSN (Fig 2) or in non-transfected SK-N-SH cells (Fig 4). These results indicate that the target of EVP4593 is upregulated in neuronal cells in response to mutant Htt^{exp} expression. In our studies we observed an excellent correlation between ability of compounds in this series to alleviate phenotype of transgenic HD flies in the climbing assay, to inhibit PMA/PHA-induced NF-κB activation in Jurkat cells and to block SOC in neuronal cells expressing Htt^{exp} (Table 1).

The molecular composition of neuronal SOC pathway is poorly understood, with potential components which include members of mammalian Trp family and Orai1 channels (Berna-Erro et al., 2009; Gruszczynska-Biegala et al., 2011; Hasan and Venkiteswaran, 2010; Putney, 2003; Venkiteswaran and Hasan, 2009). The current-voltage relationship of Isoc current in Htt138Q–transfected SK-N-SH cells (Fig 4B) was consistent with relatively non-selective Ca^{2+} channels such as Trp channels and not with highly-selective Ca^{2+} channels such as Orai1. In our experiments we demonstrated that RNAi-mediated knockdown of TRPC1 subunit significantly reduced the size of Isoc currents in Htt-138Q-transfected SK-N-SH cells (Fig 5) and in primary mouse MSN neurons (data not shown). We further demonstrated that RNAi-mediated knockdown of TRPC1 occluded ability of EVP4593 to block Isoc currents in Htt138-transfected SK-N-SH cells (Fig 5). From these experiments we concluded that TRPC1 is likely to be one of the subunit of SOC channels upregulated in response to Htt-138Q expression and inhibited by EVP4593. However, EVP4593 failed to inhibit Isoc currents supported by overexpressed TRPC1 (Fig 5). From these experiments we concluded that EVP4593 does not target TRPC1 homomeric channels but rather targets heteromeric channels containing TRPC1 as one of the subunits. Consistent with this hypothesis, we found that the levels of TRPC1 expression remain constant in Htt-138Q-transfected SK-N-SH cells (Supplementary Fig 2). Future experiments will be required to identify the subunit of SOC that is upregulated in YAC128 MSNs and in Htt-138Q-transfected cells and forms heteromeric channels with TRPC1.

These experiments suggested that the channels containing TRPC1 subunit might play a significant role in pathogenesis of HD. TRPC1 channels have been previously implicated in excitotoxic cell death of hippocampal neurons (Narayanan et al., 2008). Our conclusions are further supported by recent genetic studies. By using the same fly HD model and climbing assay as used in our study (Fig 1A) it was recently demonstrated that knockout of TRP subunit in *Drosophila* resulted in clear beneficial effects (Al-Ramahi et al., 2010). Our conclusion is also consistent with emerging role played by Trp family members in variety of neurological disorders (Selvaraj et al., 2009a; Yamamoto et al., 2007). Mutations in TRPML1 channels cause lysosomal storage neurodegenerative disorder mucolipidosis type IV (Slaugenhaupt, 2002; Venkatachalam et al., 2008). Recent studies reported that point mutations in TRPV4 channels are linked to hereditary motor and sensor neuropathies in humans (Auer-Grumbach et al., 2009; Deng et al., 2009; Landoure et al., 2009) and the gain-of-function point mutation in TRPC3 channel causes loss of cerebellar Purkinje neurons in the *moonwalker* mice (Becker et al., 2009). A potential importance of Trp channels in Parkinson's disease (PD) and in Alzheimer's disease has been also been previously discussed (Selvaraj et al., 2009a; Yamamoto et al., 2007).

To further evaluate therapeutic potential of identified compounds, we evaluated neuroprotective effects of these compounds in glutamate toxicity model with YAC128 primary MSN cultures. In the previous studies we utilized the same experimental system to evaluate potential neuroprotective effects of a number of clinically relevant compounds (Wu

et al., 2009; Wu et al., 2008; Wu et al., 2006). Based on the obtained results (Fig 6 and Table 2) we concluded that EVP4593, EVP14756 and EVP14782 exhibited neuroprotective effects in nanomolar concentrations, EVP14809 was active in micromolar concentration and EVP14808, EVP14810, and EVP14812 were inactive. Overall, there was an excellent correlation between neuroprotective effects of these compounds in YAC128 MSN glutamate toxicity model, ability of these compounds to block SOC and PMA/PHA-induced NF-kB activation, and efficacy in the climbing assay with HD flies (Table 1). We further established that Dicer RNAi-mediated knockdown of mouse TRPC1 subunit in YAC128 MSN results in significant neuroprotective effect in glutamate toxicity model (Fig 6F, Table 2). These results further supported hypothesis that TRPC1-supported SOC channels can be considered as a potential target for developing novel HD therapeutics.

Significance

The importance of store-operated Ca^{2+} entry (SOC) pathway in neuronal function is poorly understood (Hasan and Venkiteswaran, 2010; Putney, 2003). However, potential role of neuronal SOC pathway in pathological conditions has been suggested based on studies with experimental models of AD (Herms et al., 2003; Leissring et al., 2000; Yamamoto et al., 2007; Yoo et al., 2000), PD (Bollimuntha et al., 2005; Selvaraj et al., 2009b), cerebral ischemia (Berna-Erro et al., 2009) and excititoxicity (Narayanan et al., 2008). Our study together with the recent meeting report (Al-Ramahi et al., 2010) provide the first evidence that the SOC pathway may also play an important role in HD. In experiments with transgenic *Drosophila* HD model, cultured MSN neurons from YAC128 HD mouse model and SK-N-SH human neuroblastoma cells transfected with mutant Htt expression constructs we demonstrated that SOC pathway is upregulated in HD neurons. Moreover, we demonstrated that pharmacological inhibition of genetic knockdown of SOC pathway protects HD neurons from toxicity. These results provide further support to the emerging hypothesis that deranged neuronal Ca^{2+} signaling pays a key role in HD pathogenesis (Bezprozvanny, 2009). Based on our results we concluded that the TRPC1-mediated SOC pathway constitute a novel target for potential HD treatment. In addition, we identified a number of quinazoline-derived compounds (EVP4593, EVP14756 and EVP14782; Fig 1C) with ability to block neuronal SOC. These compounds can be used to dissect role of neuronal SOC in neuronal physiology. The same compounds may also provide leads for developing a novel class of therapeutic agents for treatment of HD and possibly other neurodegenerative disorders. Testing these compounds in mouse models of HD and other neurodegenerative disorders will help to evaluate future therapeutic potential of these molecules.

Experimental Procedures

Compounds

Glutamate was from Tocris. Fura-2/AM and Trichostain A (TSA) were purchased from Sigma. EVP4593 (6-amino-4-(4-phenoxyphenethyl-amino)quinazoline), EVP14782 (6-amino-4-(4- ethoxyphenethylamino)quinazoline), EVP14756 (6-amino-4-(4-n-pentyloxyphenethylamino)quinazoline), EVP14809 (4-(4-chlorophenethylamino)-6-nitroquinazoline), EVP14810 (4-3- (phenyl)propylamino)quinazoline), EVP14812 (4-(4-acetamido)-phenethylamino-6-aminoquinazoline), and EVP14808 (6-amino-4-(2-(3-pyridyl)ethylamino)-quinazoline) were previously described (Tobe et al., 2003a; Tobe et al., 2003b). The compounds were synthesized by standard organic chemistry methods (En Vivo Inc). The structures of generated compounds were confirmed by mass spectrometry and NMR analysis (En Vivo Inc). BMS-345541 was purchased from Calbiochem (Cat. No. 401480). All compounds were dissolved in DMSO as 10 mM stocks for use in animal and cellular assays.

Drosophila climbing assay

Drosophila stocks and crosses were maintained using standard procedures at 25°C, 70% relative humidity. The transgenic mutant Huntingtin line, *C(1)DX y 1 w 1118 f 1 P{w + HS-hid + }18a/P{w +mC Act5C-GFP}JMR3; P{UAS-mhtt128Q}F27B* and the pan-neuronal driver, *elav-GAL4 C155 /Y, P{w + HS-hid + }* were used to generate HD flies, *elav-GAL4 C155 /P{w +mC Act5c-GFP}JMR3; P{UAS-mhtt128Q}F27B/+* expressing first 4 exons of human Htt-128Q in the nervous system of the flies as previously described (Al-Ramahi et al., 2006). The motor function of HD flies or control flies *(UAS-LacZ* driven by *elav-GAL4* driver) were automaticaly monitored using tracking device to measure the speed of upward climbing within 7.5 seconds after dropping the flies to the bottom of the tube. This proprietary assay system and screening method have been developed by EnVivo Inc. HD flies were treated with compounds dissolved in a proprietary medium in concentration at 400 μM in the presence of 1% DMSO. Following induction of Htt-128Q transgene fragment expression, the flies were dosed daily with testing compounds and motor assays were performed. For each compound treatment, 10 flies were dispensed into each tube and assayed in triplicate. To quantify the effect of the tested compounds the difference in the average climbing speed was calculated between the groups of transgenic HD flies treated with the compound of interest and the groups treated with 1% DMSO. The difference was normalized to the standard deviation in the climbing speed determined for the entire DMSO-treated group, yielding a quantitative measure of the effect size. Statistical models indicated that in the assay conditions used (10 flies per tube, 16 tubes for one treatment and three independent experiments), effect size of 0.5 corresponds to p-value of 0.03 and the effect size of 0.8 has p-value in the range between 0.03 and 0.003. Compounds showing an effect size > 0.8 ($p < 0.003$) in the early time points (days 1–7) or an effect size >1.2 in the late time points (days 8–10) after 3 repeated assays were qualified as potential hits and evaluated further.

NF-κB assays

Human Jurkat cells (clone E6-1) were acquired from American Type Culture Collection and cultured in RPMI 1640 media (Invitrogen) supplemented with 10% FBS and 1% PS. The cells were plated at a density of 2×10^6 cells/well in 6-well dishes and transiently transfected with 1 μg/well of *pNF-kB-Luc* (Path Detect NF-κB reporter plasmid, Stratagene) using SuperFect Transfection Reagent (Qiagen). After transfection, cells were incubated for 18 hours and resuspended in RPMI 1640 medium without penicillin-streptomycin and FBS, resulting in 1.75×10^5 cells/well in the 96-well plates. Compounds were added 30 minutes before the addition of a combination of 50 ng/ml of PMA (P1585, Sigma) and 100 μg/ml of PHA (L1668, Sigma). The plates were incubated for 6 hours at 37°C and luciferase assays were performed (Bright-Glo Luciferase Assay System, Promega). Cell viability was measured by using MTS assay (Promega) to determine the compound toxicity.

SOC measurements

YAC128 mice (FVBN/NJ background strain) (Slow et al., 2003) were obtained from Jackson Labs (stock number 004938). The male YAC128 mice were crossed to wild-type (WT) female FVBN/NJ mice. P1-P2 pups were collected and genotyped by PCR. The primary cultures of MSN were established from YAC128 hemizygotous and wild-type pups as previously described (Tang et al., 2005). Briefly, striata were dissected, diced, and digested with trypsin. After dissociation, neurons were plated on poly-L-lysine (Sigma) coated, 12 mm round coverslips (Assistent) in Neurobasal-A medium supplemented with 2% B27, 1 mM of glutamine and penicillin-streptomycin (Invitrogen), and kept at 37°C in a 5% CO_2 environment.

Ca^{2+} imaging experiments with 10–14 DIV MSN cultures were performed using a DeltaRAM illuminator, an IC-300 camera, and processed by the IMAGEMASTER PRO software (PTI, Photon Technology International) as we previously described (Tang et al., 2005). Briefly, the MSN were loaded with 5 μM of Fura-2 AM for 45 min at 37°C in artificial cerebrospinal fluid containing 140 mM of NaCl, 5 mM of KCl, 1 mM of $MgCl_2$, 2 mM of $CaCl_2$, and 10 mM of Hepes pH 7.3 (ACSF). Coverslips were mounted onto a recording/perfusion chamber (RC-26G, Warner Instruments) and positioned on the movable stage of an Olympus (Melville) IX-70 inverted microscope. Images at 340 and 380 nm excitation wavelengths were acquired every 2 seconds and 340/380 Fura-2 image ratio was calculated. To determine SOC activity the cells were incubated in Ca^{2+}-free ACSF in the presence of 1 μM SERCA pump inhibitor thapsigargin for 5 min and then transferred back to ACSF containing 2 mM Ca^{2+}. The tested compounds were added to the cells 10 min prior to transfer to 2 mM Ca^{2+}.

The manganese (Mn^{2+}) quenching experiments were designed based on the published studies (Dadsetan et al., 2008; Yang et al., 2005). In these experiments the rate of Fura-2 fluorescence quenching in the presence of extracellular Mn^{2+} is used as a measure of SOC activity. The Fura-2 fluorescence was measured at isosbestic plot of 360 nm, which is not affected by changes in cytosolic Ca^{2+} concentration. For quenching experiments the cells were placed in Ca^{2+}-free ACSF and SERCA pump activity was blocked by addition of CPA. The quenching measurements were initiated by addition of 150 μM of Mn^{2+} to the extracellular media. Fura-2 fluorescent images were collected at 360 nm excitation wavelength (F_{360}) every 6 seconds. The rate of the F_{360} decline due to Fura-2 quenching is proportional to the rate of Mn^{2+} entry into the cytosol and was used as an indicator of SOC activity. The tested compounds were added to the cells 5 min after addition of Mn^{2+} solution and the rate of Fura-2 quenching was reassessed.

Electrophysiological assays

SK-N-SH human neuroblastoma cells (Cell Culture Collection, Institute of Cytology, St. Petersburg, Russia) were transiently co-transfected with Htt-15Q or Htt-138Q expression constructs and EGFP plasmid in 3:1 molar ratio as we previously described for MSN cultures (Tang et al., 2003). For TRPC1 knockdown experiments SK-N-SH cells were transiently co-transfected with a mixture of Htt-138Q expression construct, RNAi-TRPC1 plasmid and EGFP plasmid in 3:3:2 molar ratio. For TRPC1 overexpression experiments SK-N-SH cells were transiently co-transfected with a mixture of mouse TRPC1 construct in pcDNA3 expression vector (provided by Dr. Shmuel Muallem, NIH) and EGFP plasmid in 1:1. molar ratio The RNAi-TRPC1 knockdown plasmid was obtained by cloning the human TRPC1-derived sequence into pSHAG vector and it was kindly provided to us by Dr Leonidas Tsiokas (University of Oklahoma Health Sciences Center) (Bai et al., 2008). The efficiency of TRPC1 knockdown was confirmed by Western blotting of SK-N-SH cellular lysates with anti-TRPC1 polyclonal antibodies (1:200, Alomone Labs, #ACC-010). The transfected cells were identified by GFP fluorescence and the SOC currents were measured 48 h after transfection using whole-cell recordings as previously described for A431 cells (Gusev et al., 2003). Briefly, whole-cell recordings were performed using an Axopatch 200B patch clamp amplifier (Axon Instruments). Resistance of sylgard-coated, fire-polished glass microelectrodes was 3–5 MΩ. Series resistance was not compensated. The pipette solution contained (in mM) 145 NMDG aspartate, 10 Cs-EGTA, 10 Cs-HEPES pH 7.3, 1.5 $MgCl_2$, 4 Na_2ATP, 0.4 Na_2GTP and 4.8 $CaCl_2$ (pCa 7.0). Extracellular solution contained (in mM) 140 NMDG aspartate, 10 $BaCl_2$, 10 Cs-HEPES, 0.01 Tetrodotoxin (Alomone labs, Israel), 0.01 Nifedipine (Sigma Aldrich, USA) pH 7.3. For the store depletion thapsigargin (1 uM, Sigma Aldrich, USA) was used. During recording the currents were sampled at 5 kHz and filtered digitally at 500 Hz. pClamp6 software suite (Axon Instruments) was used

for data acquisition and analysis. In all whole-cell experiments the holding potential was −40 mV. Periodically (once every 5 s) the membrane potential was stepped to −100 mV (for 30 ms) and a 170 ms voltage ramp to +70 mV was applied. Traces recorded before current activation were used as a template for leak subtraction. The recorded currents were normalized to the cell capacitance. Mean value of cell capacitance was 15 ± 4 pF (n=55).

The primary cultures of striatal medium spiny neurons (MSN) were established from wild type mice pups (were collected at postnatal days 1–2) as described above for Ca^{2+} imaging experiments. Shuttle plasmid construct encoding shRNA against TRPC1 were obtained from Sigma Aldrich (MN_011643). Lenti-antiTRPC1 viruses were generated by cotransfection of shuttle vector with HIV-1 packaging vector 8.9 and VSVG envelope glycoprotein plasmids into the packaging cell line HEK293T as we previously described (Tang et al., 2009). Lenti-antiTRPC1 virus was added to MSN culture at DIV6 and the whole-cell patch-clamp recordings of currents in cultured DIV10 MSN were performed according to procedures described for SK-N-SH cells with addition of 10 mM Glucose to the extracellular solution

YAC128 MSN glutamate toxicity assay

The assay for glutamate-induced cell death was performed with primary WT and YAC128 MSN as we previously described (Tang et al., 2005). The primary cultures were established as described above. Test compounds were added at 14 DIV (days *in vitro*) to WT and YAC128 MSN cultures at the final concentration of 0.03 μM, 0.3 μM and 3.0 μM from DMSO stocks as indicated. In parallel control experiments the cultures were exposed to 1‰ DMSO. After 30 min incubation with the test compounds, the MSN were exposed for 7 hours to 250 μM of glutamate added to the culture medium. Immediately after the treatment with glutamate, neurons were fixed for 30 min in 4% formaldehyde plus 4% sucrose in PBS (pH7.4), permeabilized for 5 min in 0.25% Triton-X-100, and stained by using the DeadEnd fluorometric TUNEL System (Promega). Nuclei were counterstained with 5 μM of propidium iodine (PI) (Molecular Probes). Coverslips were extensively washed with PBS and mounted in Mowiol 4–88 (Polysciences). Six to eight randomly chosen microscopic fields containing 100–300 MSN each were manually counted using Olympus IX70 fluorescent microscope. The number of TUNEL-positive neuronal nuclei was calculated as a fraction of PI-positive neuronal nuclei in each microscopic field. The fractions of TUNEL-positive nuclei determined for each microscopic field were averaged and the results are presented as means ± SE (n= number of fields counted).

Dicer-mediated approach was used to achieve siRNA knockdown of TRPC1 in primary MSN cultures by following described procedures (Supnet et al., 2006). Full-length mouse TRPC1 cDNA was obtained from Open Biosystems (clone ID 8860600) and used as a PCR template to amplify a 300 bp fragment (bp 2102– 2401 in mouse TRPC1). T7 promoter sequence was included in the sequence of both forward and reverse primers as follows: FP = TAATACGACTCACTATAGGGTTCCTTCTCCAAAGA, RP = TAATACGACTCACTATAGGGTAGAAGTCCGAAAGC. The product of PCR reaction was purified by NucleoSpin Extract II (Clontech) and dsRNA was obtained by T7 polymerase-mediated transcription for 16h at 37°C (TurboScript T7 Transcription Kit, Genlantis) followed by DNase I digestion for 15 min at 37°C. dsRNA was purified by lithium chloride precipitation and quantified using NanoDrop 2000c (Thermo Scientific). Four microgram dsRNA and four unit of recombinant PowerCut Dicer enzyme (Finnzymes) were combined with PowerCut Dicer Reaction Buffer in a total volume of 20 μl. After 16h at 37°C, dsiRNA was purified on two consecutive RNA purification columns to remove salts and free nucleotides. Described procedure yielded a size-homogeneous population < 30 bp dsiRNA without contaminating long dsRNA. Concentration of dsiRNA was determined by NanoDrop 2000c. The WT and YAC128 MSN cultures were transfected on DIV2–4 by a mixture of 275 ng siRNA-TRPC1 and 1 μM Accell Fluorescently-labeled non-targeting siRNA reagent

(Thermo Scientific Dharmacon) using Polyethylenimine (PEI) transfection reagent. The same amount of non-targeting siRNA reagent was used in control transfections (Ctrl-siRNA). In both cases the neuronal transfection efficiency was at least 80%, consistent with the previous studies (Supnet et al., 2006). On DIV14, the MSN were exposed for 7 hours to 250 μM of glutamate added to the culture medium and then were fixed and permeablizied as described above. The neurons were stained using In Situ Cell Death Detection Kit, TMR red (Roche). Nuclei were counterstained with 3 μM of 4'-6-Diamidino-2-phenylindole (DAPI). Six to eight randomly chosen microscopic fields containing 100–300 MSN each were manually counted. The number of TUNEL-positive neuronal nuclei was calculated as a fraction of DAPI-positive neuronal nuclei in each microscopic field. The fractions of TUNEL-positive nuclei determined for each microscopic field were averaged and the results are presented as means ± SE (n= number of fields counted).

Statistical analysis

All experiments were repeated for at least three times. Data were evaluated for statistical significance by analysis using SigmaPlot t-test or One-Way ANOVA. Statistical difference was considered to be significant only if $p<0.05$.

Highlights

1. Discovered that store-operated Ca^{2+} entry (SOC) pathway is enhanced in Huntington's disease (HD) neurons.
2. Identified a novel class of quinazoline-derived compounds that inhibit SOC pathway in HD neurons.
3. Demonstrated that the identified compounds exert neuroprotective effects in studies with transgenic HD flies and transgenic HD mouse neurons.
4. Established key role of TRPC1 channels in supporting SOC pathway in HD neurons.

Supplementary Material

Refer to Web version on PubMed Central for supplementary material.

Acknowledgments

We thank Juan Botas (Baylor Univ) for generously providing us transgenic mhtt128 HD flies that were used to generate the stocks in this study, Leonidas Tsiokas (University of Oklahoma Health Sciences Center) for a gift of human TRPC1-RNAi plasmid, Yuemei Li and Huarui Liu for help with maintaining the YAC128 mouse colony and genotyping, Leah Benson for administrative assistance, Tie-Shan Tang for helpful advice and discussions, Gerhard Koenig (EnVivo) for comments on the manuscript. IB is a holder of Carl J. and Hortense M. Thomsen chair in Alzheimer's disease research. The study was supported by EnVivo Inc, CHDI foundation, and the NINDS R01 NS056224 (IB), the Program of Ministry of Science and Education GCs N 14.740.11.0924 (IB and EK) and N P332 (EK), Russian Basic Research Foundation 10-04-00956 (EK).

References

Al-Ramahi, I.; Kim, E.; SANHUEZA, M.; DIAZ, J.; Botas, J. Screen of genes involved in Ca2+ homeostasis and signaling to identify genetic modifiers and potential therapeutic targets for Huntington's Disease treatment. Paper presented at: Society for Neuroscience; San Diego. 2010.

Al-Ramahi I, Lam YC, Chen HK, de Gouyon B, Zhang M, Perez AM, Branco J, de Haro M, Patterson C, Zoghbi HY, et al. CHIP protects from the neurotoxicity of expanded and wild-type ataxin-1 and promotes their ubiquitination and degradation. J Biol Chem. 2006; 281:26714–26724. [PubMed: 16831871]

Auer-Grumbach M, Olschewski A, Papic L, Kremer H, McEntagart ME, Uhrig S, Fischer C, Frohlich E, Balint Z, Tang B, et al. Alterations in the ankyrin domain of TRPV4 cause congenital distal SMA, scapuloperoneal SMA and HMSN2C. Nat Genet. 2009

Bai CX, Giamarchi A, Rodat-Despoix L, Padilla F, Downs T, Tsiokas L, Delmas P. Formation of a new receptor-operated channel by heteromeric assembly of TRPP2 and TRPC1 subunits. EMBO Rep. 2008; 9:472–479. [PubMed: 18323855]

Becker EB, Oliver PL, Glitsch MD, Banks GT, Achilli F, Hardy A, Nolan PM, Fisher EM, Davies KE. A point mutation in TRPC3 causes abnormal Purkinje cell development and cerebellar ataxia in moonwalker mice. Proc Natl Acad Sci U S A. 2009; 106:6706–6711. [PubMed: 19351902]

Berna-Erro A, Braun A, Kraft R, Kleinschnitz C, Schuhmann MK, Stegner D, Wultsch T, Eilers J, Meuth SG, Stoll G, et al. STIM2 regulates capacitive Ca2+ entry in neurons and plays a key role in hypoxic neuronal cell death. Sci Signal. 2009; 2:ra67. [PubMed: 19843959]

Bezprozvanny I. Calcium signaling and neurodegenerative diseases. Trends Mol Med. 2009; 15:89–100. [PubMed: 19230774]

Bollimuntha S, Singh BB, Shavali S, Sharma SK, Ebadi M. TRPC1-mediated inhibition of 1-methyl-4-phenylpyridinium ion neurotoxicity in human SH-SY5Y neuroblastoma cells. J Biol Chem. 2005; 280:2132–2140. [PubMed: 15542611]

Bootman MD, Collins TJ, Mackenzie L, Roderick HL, Berridge MJ, Peppiatt CM. 2-aminoethoxydiphenyl borate (2-APB) is a reliable blocker of store-operated Ca2+ entry but an inconsistent inhibitor of InsP3-induced Ca2+ release. Faseb J. 2002; 16:1145–1150. [PubMed: 12153982]

Burke JR, Pattoli MA, Gregor KR, Brassil PJ, MacMaster JF, McIntyre KW, Yang X, Iotzova VS, Clarke W, Strnad J, et al. BMS-345541 is a highly selective inhibitor of I kappa B kinase that binds at an allosteric site of the enzyme and blocks NF-kappa B-dependent transcription in mice. J Biol Chem. 2003; 278:1450–1456. [PubMed: 12403772]

Cha JH. Transcriptional signatures in Huntington's disease. Prog Neurobiol. 2007; 83:228–248. [PubMed: 17467140]

Chen N, Luo T, Wellington C, Metzler M, McCutcheon K, Hayden MR, Raymond LA. Subtype-specific enhancement of NMDA receptor currents by mutant huntingtin. J Neurochem. 1999; 72:1890–1898. [PubMed: 10217265]

Choi S, Kim JH, Roh EJ, Ko MJ, Jung JE, Kim HJ. Nuclear factor-kappaB activated by capacitative Ca2+ entry enhances muscarinic receptor-mediated soluble amyloid precursor protein (sAPPalpha) release in SH-SY5Y cells. J Biol Chem. 2006; 281:12722–12728. [PubMed: 16490783]

Choo YS, Johnson GV, MacDonald M, Detloff PJ, Lesort M. Mutant huntingtin directly increases susceptibility of mitochondria to the calcium-induced permeability transition and cytochrome c release. Hum Mol Genet. 2004; 13:1407–1420. [PubMed: 15163634]

Chu CT, Plowey ED, Wang Y, Patel V, Jordan-Sciutto KL. Location, location, location: altered transcription factor trafficking in neurodegeneration. J Neuropathol Exp Neurol. 2007; 66:873–883. [PubMed: 17917581]

Clapham DE, Runnels LW, Strubing C. The TRP ion channel family. Nat Rev Neurosci. 2001; 2:387–396. [PubMed: 11389472]

Dadsetan S, Zakharova L, Molinski TF, Fomina AF. Store-operated Ca2+ influx causes Ca2+ release from the intracellular Ca2+ channels that is required for T cell activation. J Biol Chem. 2008; 283:12512–12519. [PubMed: 18316371]

Deng HX, Klein CJ, Yan J, Shi Y, Wu Y, Fecto F, Yau HJ, Yang Y, Zhai H, Siddique N, et al. Scapuloperoneal spinal muscular atrophy and CMT2C are allelic disorders caused by alterations in TRPV4. Nat Genet. 2009

Desai UA, Pallos J, Ma AA, Stockwell BR, Thompson LM, Marsh JL, Diamond MI. Biologically active molecules that reduce polyglutamine aggregation and toxicity. Hum Mol Genet. 2006; 15:2114–2124. [PubMed: 16720620]

Fan MM, Fernandes HB, Zhang LY, Hayden MR, Raymond LA. Altered NMDA receptor trafficking in a yeast artificial chromosome transgenic mouse model of Huntington's disease. J Neurosci. 2007; 27:3768–3779. [PubMed: 17409241]

Gil JM, Rego AC. Mechanisms of neurodegeneration in Huntington's disease. Eur J Neurosci. 2008; 27:2803–2820. [PubMed: 18588526]

Gruszczynska-Biegala J, Pomorski P, Wisniewska MB, Kuznicki J. Differential Roles for STIM1 and STIM2 in Store-Operated Calcium Entry in Rat Neurons. PLOS One. 2011 *in press*.

Gusev K, Glouchankova L, Zubov A, Kaznacheyeva E, Wang Z, Bezprozvanny I, Mozhayeva GN. The store-operated calcium entry pathways in human carcinoma A431 cells: functional properties and activation mechanisms. J Gen Physiol. 2003; 122:81–94. [PubMed: 12835472]

Hasan G, Venkiteswaran G. The enigma of store-operated ca-entry in neurons: answers from the Drosophila flight circuit. Front Neural Circuits. 2010; 4:10. [PubMed: 20407638]

Herms J, Schneider I, Dewachter I, Caluwaerts N, Kretzschmar H, Van Leuven F. Capacitive calcium entry is directly attenuated by mutant presenilin-1, independent of the expression of the amyloid precursor protein. J Biol Chem. 2003; 278:2484–2489. [PubMed: 12431992]

HSG. Tetrabenazine as antichorea therapy in Huntington disease: a randomized controlled trial. Neurology. 2006; 66:366–372. [PubMed: 16476934]

Imarisio S, Carmichael J, Korolchuk V, Chen CW, Saiki S, Rose C, Krishna G, Davies JE, Ttofi E, Underwood BR, et al. Huntington's disease: from pathology and genetics to potential therapies. Biochem J. 2008; 412:191–209. [PubMed: 18466116]

Khoshnan A, Ko J, Watkin EE, Paige LA, Reinhart PH, Patterson PH. Activation of the IkappaB kinase complex and nuclear factor-kappaB contributes to mutant huntingtin neurotoxicity. J Neurosci. 2004; 24:7999–8008. [PubMed: 15371500]

Landoure G, Zdebik AA, Martinez TL, Burnett BG, Stanescu HC, Inada H, Shi Y, Taye AA, Kong L, Munns CH, et al. Mutations in TRPV4 cause Charcot-Marie-Tooth disease type 2C. Nat Genet. 2009

Leissring MA, Akbari Y, Fanger CM, Cahalan MD, Mattson MP, LaFerla FM. Capacitative calcium entry deficits and elevated luminal calcium content in mutant presenilin-1 knockin mice. J Cell Biol. 2000; 149:793–798. [PubMed: 10811821]

Ma HT, Venkatachalam K, Rys-Sikora KE, He LP, Zheng F, Gill DL. Modification of phospholipase C-gamma-induced Ca2+ signal generation by 2-aminoethoxydiphenyl borate. Biochem J. 2003; 376:667–676. [PubMed: 14558886]

Marsh JL, Lukacsovich T, Thompson LM. Animal models of polyglutamine diseases and therapeutic approaches. J Biol Chem. 2009; 284:7431–7435. [PubMed: 18957429]

Milnerwood AJ, Raymond LA. Corticostriatal synaptic function in mouse models of Huntington's disease: early effects of huntingtin repeat length and protein load. J Physiol. 2007; 585:817–831. [PubMed: 17947312]

Montell C. The TRP superfamily of cation channels. Sci STKE. 2005:re3. [PubMed: 15728426]

Nakai M, Qin ZH, Chen JF, Wang Y, Chase TN. Kainic acid-induced apoptosis in rat striatum is associated with nuclear factor-kappaB activation. J Neurochem. 2000; 74:647–658. [PubMed: 10646516]

Narayanan KL, Irmady K, Subramaniam S, Unsicker K, von Bohlen und Halbach O. Evidence that TRPC1 is involved in hippocampal glutamate-induced cell death. Neurosci Lett. 2008; 446:117–122. [PubMed: 18822346]

Panov AV, Gutekunst CA, Leavitt BR, Hayden MR, Burke JR, Strittmatter WJ, Greenamyre JT. Early mitochondrial calcium defects in Huntington's disease are a direct effect of polyglutamines. Nat Neurosci. 2002; 5:731–736. [PubMed: 12089530]

Petrucelli L, Dawson TM. Mechanism of neurodegenerative disease: role of the ubiquitin proteasome system. Ann Med. 2004; 36:315–320. [PubMed: 15224658]

Putney JW Jr. Capacitative calcium entry in the nervous system. Cell Calcium. 2003; 34:339–344. [PubMed: 12909080]

Qin ZH, Wang Y, Chen RW, Wang X, Ren M, Chuang DM, Chase TN. Prostaglandin A(1) protects striatal neurons against excitotoxic injury in rat striatum. J Pharmacol Exp Ther. 2001; 297:78–87. [PubMed: 11259530]

Qin ZH, Wang Y, Nakai M, Chase TN. Nuclear factor-kappa B contributes to excitotoxin-induced apoptosis in rat striatum. Mol Pharmacol. 1998; 53:33–42. [PubMed: 9443930]

Ravikumar B, Vacher C, Berger Z, Davies JE, Luo S, Oroz LG, Scaravilli F, Easton DF, Duden R, O'Kane CJ, et al. Inhibition of mTOR induces autophagy and reduces toxicity of polyglutamine expansions in fly and mouse models of Huntington disease. Nat Genet. 2004; 36:585–595. [PubMed: 15146184]

Riccio A, Medhurst AD, Mattei C, Kelsell RE, Calver AR, Randall AD, Benham CD, Pangalos MN. mRNA distribution analysis of human TRPC family in CNS and peripheral tissues. Brain Res Mol Brain Res. 2002; 109:95–104. [PubMed: 12531519]

Roze E, Saudou F, Caboche J. Pathophysiology of Huntington's disease: from huntingtin functions to potential treatments. Curr Opin Neurol. 2008; 21:497–503. [PubMed: 18607213]

Selvaraj S, Sun Y, Singh BB. TRPC Channels and their Implication in Neurological Diseases. CNS Neurol Disord Drug Targets. 2009a

Selvaraj S, Watt JA, Singh BB. TRPC1 inhibits apoptotic cell degeneration induced by dopaminergic neurotoxin MPTP/MPP(+). Cell Calcium. 2009b; 46:209–218. [PubMed: 19695701]

Slaugenhaupt SA. The molecular basis of mucolipidosis type IV. Curr Mol Med. 2002; 2:445–450. [PubMed: 12125810]

Slow EJ, van Raamsdonk J, Rogers D, Coleman SH, Graham RK, Deng Y, Oh R, Bissada N, Hossain SM, Yang YZ, et al. Selective striatal neuronal loss in a YAC128 mouse model of Huntington disease. Hum Mol Genet. 2003; 12:1555–1567. [PubMed: 12812983]

Steffan JS, Bodai L, Pallos J, Poelman M, McCampbell A, Apostol BL, Kazantsev A, Schmidt E, Zhu YZ, Greenwald M, et al. Histone deacetylase inhibitors arrest polyglutamine-dependent neurodegeneration in Drosophila. Nature. 2001; 413:739–743. [PubMed: 11607033]

Sugars KL, Brown R, Cook LJ, Swartz J, Rubinsztein DC. Decreased cAMP response element-mediated transcription: an early event in exon 1 and full-length cell models of Huntington's disease that contributes to polyglutamine pathogenesis. J Biol Chem. 2004; 279:4988–4999. [PubMed: 14627700]

Sun Y, Savanenin A, Reddy PH, Liu YF. Polyglutamine-expanded huntingtin promotes sensitization of N-methyl-D- aspartate receptors via post-synaptic density 95. J Biol Chem. 2001; 276:24713–24718. [PubMed: 11319238]

Supnet C, Grant J, Kong H, Westaway D, Mayne M. Amyloid-beta-(1–42) increases ryanodine receptor-3 expression and function in neurons of TgCRND8 mice. J Biol Chem. 2006; 281:38440–38447. [PubMed: 17050533]

Tang TS, Guo C, Wang H, Chen X, Bezprozvanny I. Neuroprotective effects of inositol 1,4,5-trisphosphate receptor C-terminal fragment in a Huntington's disease mouse model. J Neurosci. 2009; 29:1257–1266. [PubMed: 19193873]

Tang TS, Slow E, Lupu V, Stavrovskaya IG, Sugimori M, Llinas R, Kristal BS, Hayden MR, Bezprozvanny I. Disturbed Ca2+ signaling and apoptosis of medium spiny neurons in Huntington's disease. Proc Natl Acad Sci U S A. 2005; 102:2602–2607. [PubMed: 15695335]

Tang TS, Tu H, Chan EY, Maximov A, Wang Z, Wellington CL, Hayden MR, Bezprozvanny I. Huntingtin and huntingtin-associated protein 1 influence neuronal calcium signaling mediated by inositol-(1,4,5) triphosphate receptor type 1. Neuron. 2003; 39:227–239. [PubMed: 12873381]

The., Huntington's., Disease., Collaborative., Research., Group. A novel gene containing a trinucleotide repeat that is expanded and unstable on Huntington's disease chromosomes. Cell. 1993; 72:971–983. [PubMed: 8458085]

Thompson LM, Aiken CT, Kaltenbach LS, Agrawal N, Illes K, Khoshnan A, Martinez-Vincente M, Arrasate M, O'Rourke JG, Khashwji H, et al. IKK phosphorylates Huntingtin and targets it for degradation by the proteasome and lysosome. J Cell Biol. 2009; 187:1083–1099. [PubMed: 20026656]

Tobe M, Isobe Y, Tomizawa H, Nagasaki T, Takahashi H, Fukazawa T, Hayashi H. Discovery of quinazolines as a novel structural class of potent inhibitors of NF-kappa B activation. Bioorg Med Chem. 2003a; 11:383–391. [PubMed: 12517433]

Tobe M, Isobe Y, Tomizawa H, Nagasaki T, Takahashi H, Hayashi H. A novel structural class of potent inhibitors of NF-kappa B activation: structure-activity relationships and biological effects of 6-aminoquinazoline derivatives. Bioorg Med Chem. 2003b; 11:3869–3878. [PubMed: 12927847]

Venkatachalam K, Long AA, Elsaesser R, Nikolaeva D, Broadie K, Montell C. Motor deficit in a Drosophila model of mucolipidosis type IV due to defective clearance of apoptotic cells. Cell. 2008; 135:838–851. [PubMed: 19041749]

Venkiteswaran G, Hasan G. Intracellular Ca2+ signaling and store-operated Ca2+ entry are required in Drosophila neurons for flight. Proc Natl Acad Sci U S A. 2009; 106:10326–10331. [PubMed: 19515818]

Vonsattel JP, DiFiglia M. Huntington disease. J Neuropathol Exp Neurol. 1998; 57:369–384. [PubMed: 9596408]

Wenning AS, Neblung K, Strauss B, Wolfs MJ, Sappok A, Hoth M, Schwarz EC. TRP expression pattern and the functional importance of TRPC3 in primary human T-cells. Biochim Biophys Acta. 2011

Wu J, Jeong HK, Bulin SE, Kwon SW, Park JH, Bezprozvanny I. Ginsenosides protect striatal neurons in a cellular model of Huntington's disease. J Neurosci Res. 2009; 87:1904–1912. [PubMed: 19185022]

Wu J, Li Q, Bezprozvanny I. Evaluation of Dimebon in cellular model of Huntington's disease. Mol Neurodegener. 2008; 3:15. [PubMed: 18939977]

Wu J, Tang T, Bezprozvanny I. Evaluation of clinically relevant glutamate pathway inhibitors in in vitro model of Huntington's disease. Neurosci Lett. 2006; 407:219–223. [PubMed: 16959411]

Yamamoto S, Wajima T, Hara Y, Nishida M, Mori Y. Transient receptor potential channels in Alzheimer's disease. Biochim Biophys Acta. 2007; 1772:958–967. [PubMed: 17490865]

Yang KT, Chen WP, Chang WL, Su MJ, Tsai KL. Arachidonic acid inhibits capacitative Ca2+ entry and activates non-capacitative Ca2+ entry in cultured astrocytes. Biochem Biophys Res Commun. 2005; 331:603–613. [PubMed: 15850803]

Yoo AS, Cheng I, Chung S, Grenfell TZ, Lee H, Pack-Chung E, Handler M, Shen J, Xia W, Tesco G, et al. Presenilin-mediated modulation of capacitative calcium entry. Neuron. 2000; 27:561–572. [PubMed: 11055438]

Zeron MM, Hansson O, Chen N, Wellington CL, Leavitt BR, Brundin P, Hayden MR, Raymond LA. Increased sensitivity to N-methyl-D-aspartate receptor-mediated excitotoxicity in a mouse model of Huntington's disease. Neuron. 2002; 33:849–860. [PubMed: 11906693]

Zhang H, Li Q, Graham RK, Slow E, Hayden MR, Bezprozvanny I. Full length mutant huntingtin is required for altered Ca2+ signaling and apoptosis of striatal neurons in the YAC mouse model of Huntington's disease. Neurobiol Dis. 2008; 31:80–88. [PubMed: 18502655]

Zhang Y, Leavitt BR, van Raamsdonk JM, Dragatsis I, Goldowitz D, MacDonald ME, Hayden MR, Friedlander RM. Huntingtin inhibits caspase-3 activation. Embo J. 2006; 25:5896–5906. [PubMed: 17124493]

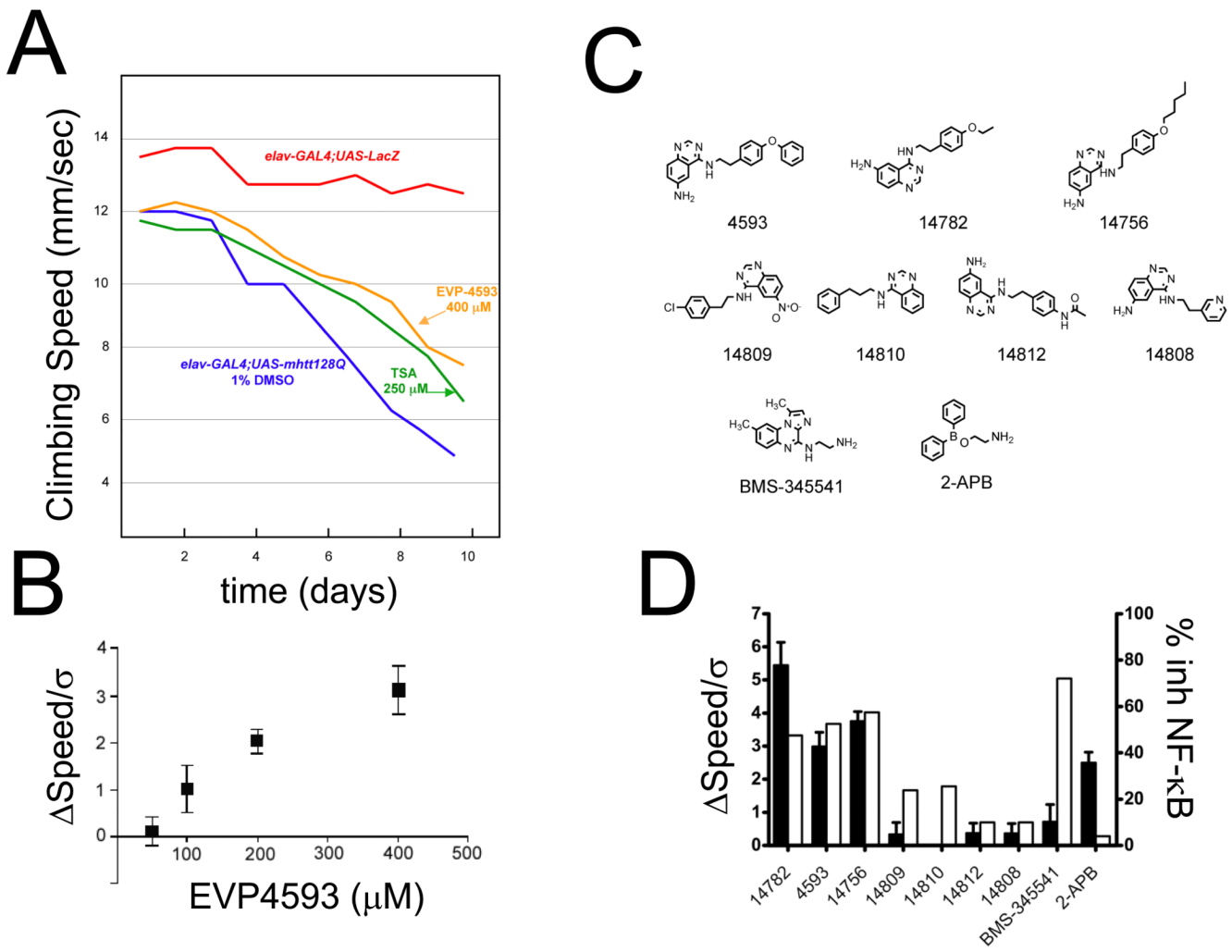

Figure 1. Identification of EVP4593 in climbing assay screen with HD transgenic flies

(A) The climbing speed of HD flies is plotted as a function of time following induction of mHtt-128Q transgene. The results with lacZ –expressing flies are shown as a control (red). A number of small molecule compounds were dissolved in DMSO and included in the fly food in the final concentration as indicated. The results obtained in HD flies for 400 μM EVP4593 (orange), 250 μM TSA (green) and 1% DMSO (blue) are compared.

(B) Dose-dependence of EVP4593 in rescuing motor dysfunction of HD flies. An average effect size relative to 1% DMSO control was determined at days 8–10 after mHtt-128Q transgene induction (ΔSpeed), normalized to variability of the climbing speed in DMSO-treated group (σ) and plotted as mean ± S.E. (n = 30 flies) against concentration of EVP4593 in the fly food.

(C) Chemical structures of EVP4593 and its analogues used in the study. BMS-345541 is an unrelated compound with potent IKK inhibitory activity. 2-APB is an unrelated compound with ability to block SOC with low affinity in some cell types.

(D) The potency of 200 μM of EVP4593 or its analogs in the climbing assay was determined as an average effect size at days 8–10 after mHtt-128Q transgene induction and shown as mean ± S.E. (n = 30 flies) (filled bars). The potency of 1 μM of EVP4593 or its analogs was determined as % inhibition of NF-κB activity and shown as mean ± S.E. (n = 4–

6) (open bars). Also shown are results for BMS-345541 and 2-APB (400 μM in climbing assay and 1 μM in NF-κB assay for both compounds)
See also Figure S1.

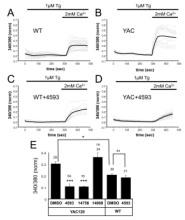

Figure 2. SOC pathway in WT and YAC128 MSNs - Ca^{2+} imaging assay

(A, B) WT (A) and YAC128 (B) MSN cultures at DIV10–14 were loaded with Fura-2 Ca^{2+} imaging dye and incubated in Ca^{2+}-free media. The intracellular Ca^{2+} stores were depleted by addition of 1 μM of thapsigargin (Tg) as indicated. Readdition of 2 mM Ca^{2+} to the extracellular media resulted in Ca^{2+} influx via SOC pathway. Fura-2 340/380 ratio traces are shown for individual cells (gray thin lines). For each cell 340/380 ratio trace was offset to 0.0 for the time point of Ca^{2+} re-addition. The average trace is also shown (black thick line). (C,D). SOC Ca^{2+} imaging experiments were performed with WT (C) and YAC128 (D) MSN in the presence of 300 nM EVP4593.

(E). An average amplitude of an increase in 340/380 Fura-2 signals in response to Ca^{2+} readdition is shown for YAC128 and WT MSN in the presence of DMSO or 300 nM of test compounds as indicated. The results are shown as mean ± S.E. (number of cells is shown on the top of the bar). *, $p < 0.05$; ***, $p<0.001$ when compared to DMSO group.

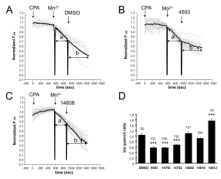

Figure 3. SOC pathway in YAC128 MSNs - Mn^{2+} quenching assay

(A–C). SOC pathway in YAC128 MSN is quantified by Mn^{2+} quenching assay. The YAC128 MSNs loaded with Fura-2 were placed in Ca^{2+} -free and Mn^{2+}-free media containing 100 μM EGTA. The intracellular Ca^{2+} stores are depleted by 10 min incubation with 30 μM of CPA. Following addition of 150 μM of Mn^{2+} to the extracellular media the Fura-2 quenching is quantified as reduction of the Fura-2 fluorescent signal at isobestic λ_{ex} = 360 nM (F_{360}). The rate of Fura-2 Mn^2 quenching is calculated as the slope of the curve and determined for each cell before (phase a) and after (phase b) addition of DMSO (A), 300 nM of EVP4593 (B) or 300 nM EVP14808 (C). Fura-2 F_{360} traces are shown for individual cells (gray thin lines). For each cell F_{360} signal was normalized to F_{360} signal at the time point of Mn^{2+} addition. The average trace is also shown (black thick line). (D) The changes in Fura-2 Mn^{2+} quench rates in YAC128 MSNs are plotted as b/a slope ratios for each compound tested at 300 nM concentration. The average b/a ratios for each compound are shown as mean ± S.E. (number of cells is indicated above each bar). ***, $p<0.001$ when compared to DMSO group.

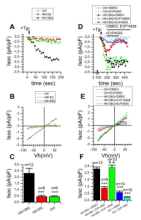

Figure 4. Recordings of Isoc in SK-N-SH cells transfected with Htt-15Q and Htt-138Q

(A) The amplitude of Isoc currents recorded in whole-cell experiments are shown as a function of time after application of 1 μM Tg (indicated by arrow) to non-transfected SK-N-SH cells (Ctrl, green triangles) and to SK-N-SH cells transiently transfected with Htt-15Q (red squares) or Htt-138Q (black circles). The amplitude of Isoc currents for all groups of cells was measured every 10 seconds at −80 mV test potential. Data from representative experiments are shown.

(B) The average current-voltage relationships recorded after full development of Isoc in non-transfected SK-N-SH cells (Ctrl, green trace) and SK-N-SH transiently transfected with Htt-15Q (red trace), or Htt-138Q (black trace). Each trace is an average based on a number of experiments as indicated in panel C.

(C) The average Isoc amplitude in non-transfected SK-N-SH cells (Ctrl) and in SK-N-SH transfected with Htt-15Q or Htt-138Q constructs. For all groups of cells Isoc amplitude was determined at −80 mV test potential and plotted as mean ± SE (n = number of experiments). ***, $p<0.001$ when compared to Htt138Q-transfected cells..

(D) Isoc currents in non-transfected SK-N-SH cells (Ctrl) and SK-N-SH cells transfected with Htt-138Q plasmid are shown as a function of the time after 1 μM Tg application (indicated by arrow). The representative data obtained in the presence of DMSO (blue triangles for non-transfected cells and black circles for transfected cells), 300 nM EVP4593 (red squares for transfected cells and cyan rhombs for non-transfected cells) and 300 nM EVP14808 (green triangles for transfected cells) are shown. The amplitude of Isoc currents for all groups of cells was measured every 10 seconds at −80 mV test potential. The times of EVP4593, EVP14808 and DMSO applications are shown above the Isoc plot.

(E) The average current-voltage relationships recorded after full development of Isoc in non-transfected SK-N-SH cells (Ctrl) and in SK-N-SH transfected with Htt-138Q in the presence of DMSO (blue trace for control cells and black trace for transfected cells), 300 nM EVP4593 (cyan trace for control cells and red trace for transfected cells), and 300 nM EVP14808 (green trace). Each trace is an average based on a number of experiments indicated in panel F.

(F) The average Isoc amplitude in non-transfected (Ctrl) SK-N-SH cells and in SK-N-SH cells transfected with Htt-138 and recorded in the presence of DMSO, 300 nM EVP4593 or 300 nM EVP14808. For all groups of cells Isoc amplitude was determined at −80 mV test potential and plotted as mean ± SE (n = number of experiments). ***, $p<0.001$ when compared to Htt138Q-transfected cells in the presence of DMSO.

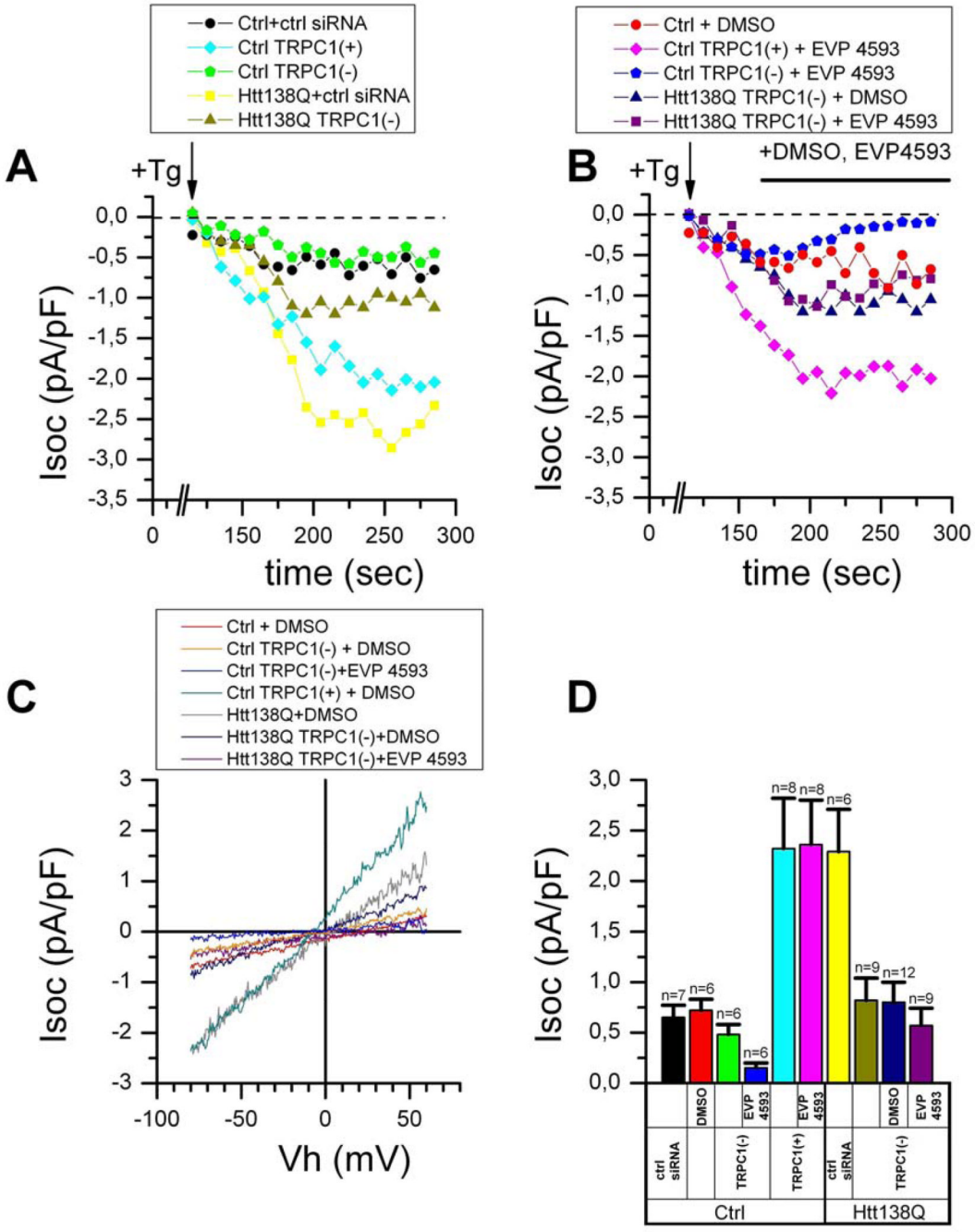

Figure 5. TRPC1 supports Isoc currents in SK-N-SH cells transfected with Htt-138Q

(A) The amplitude of Isoc currents recorded in whole-cell experiments is shown as a function of time after application of 1 μM Tg (indicated by arrow) to SK-N-SH cells transiently transfected with scrambled siRNA (Ctrl+ctrl siRNA, black circles), to SK-N-SH cells transiently transfected with TRPC1 plasmid (Ctrl TRPC1+, cyan rhombs), to SK-N-SH cells transiently transfected with TRPC1-RNAi (Ctrl TRPC1-, green pentagons), to SK-N-SH cells transiently co-transfected with Htt-138Q and scrambled siRNA (yellow squares) or to SK-N-SH cells co-transfected with Htt-138Q and TRPC1-RNAi (dark yellow triangles). (B) The amplitude of Isoc currents recorded in whole-cell experiments are shown as a function of time after application of 1 μM Tg (indicated by arrow) to non-transfected SK-N-

SH cells treated with DMSO (Ctrl, red circles), to SK-N-SH cells transiently transfected with TRPC1 and treated with 300 nM EVP4593 (Ctrl TRPC1+, pink rhombs), to SK-N-SH cells transiently transfected with TRPC1-RNAi and treated with 300 nM EVP4593 (Ctrl TRPC1-, blue pentagons), to SK-N-SH cells co-transfected with Htt-138Q and TRPC1-RNAi and treated with DMSO (navy triangles) or to SK-N-SH cells co-transfected with Htt-138Q and TRPC1-RNAi and treated with 300 nM EVP4593 (purple squares). The times of EVP4593 and DMSO applications are shown above the Isoc plot.

On panels A and B the amplitude of the Isoc currents for all groups of cells was measured every 10 seconds at −80 mV test potential. Data from representative experiments are shown for each group of cells.

(C) The average current-voltage relationships recorded after full development of Isoc in non-transfected SK-N-SH cells (Ctrl, red trace), in SK-N-SH cells transfected with TRPC1-RNAi and treated with DMSO (yellow trace) or 300 nM EVP4593 (blue trace), in SK-N-SH cells transfected with Htt-138Q and treated with DMSO (black trace),), in SK-N-SH cells transfected with TRPC1 and treated with DMSO (gray trace), in SK-N-SH cells co-transfected with Htt-138Q and TRPC1-RNAi and treated with DMSO (navy trace), and in SK-N-SH cells co-transfected with Htt-138Q and TRPC1-RNAi and treated with 300 nM EVP4593 (purple trace). Each trace is an average based on a number of experiments indicated in panel D.

(D) The average Isoc amplitude in SK-N-SH cells transfected with scrambled siRNA, in non-transfected SK-N-SH cells treated with DMSO, in SK-N-SH cells transfected with TRPC1-RNAi with and without treatment with 300 nM EVP4593, in SK-N-SH cells transfected with TRPC1-cDNA with and without treatment with 300 nM EVP4593, in SK-N-SH cells co-transfected with Htt-138Q and scrambled siRNA, and in SK-N-SH cells co-transfected with Htt-138Q and TRPC1-RNAi untreated, treated with DMSO or treated with 300 nM EVP4593. For all groups of cells Isoc amplitude was determined at −80 mV test potential and plotted as mean ± SE (n = number of experiments).

See also Figure S2.

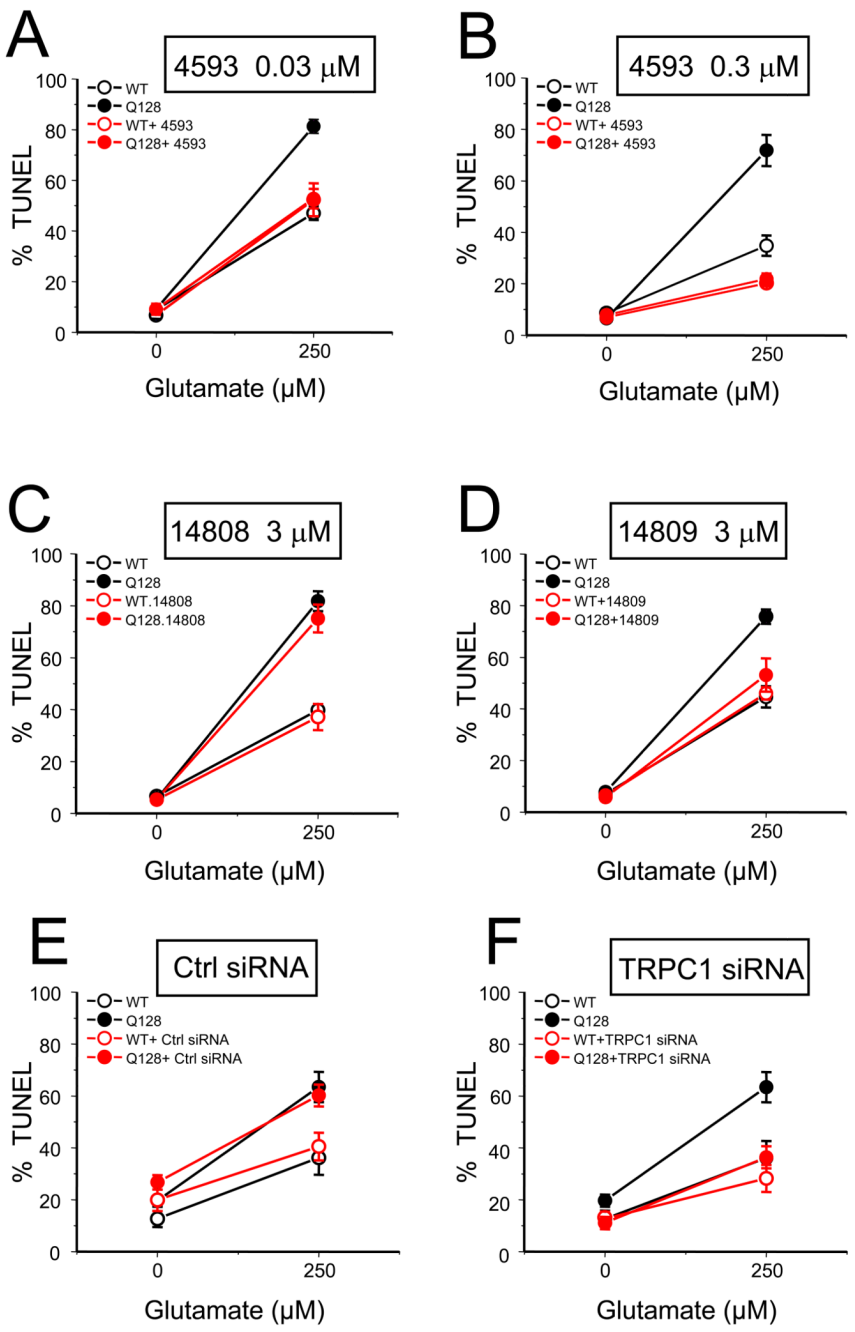

Figure 6. Compounds from EVP4593 series or knockdown of TRPC1 protect YAC128 MSNs from glutamate-induced apoptosis

The fraction of TUNEL-positive nuclei is plotted against glutamate concentration for MSN from WT (open circle) and YAC128 (YAC, filled circles) mice. The results in the absence (black symbols) and presence (red symbols) of compounds or treatments are compared. The data are shown for (A) 0.03 μM of EVP4593; (B) 0.3 μM of EVP4593; (C) 3 μM of EVP14808; (D) 3 μM of EVP14809; (E) treatment with non-targeting RNAi reagent; (F) treatment with TRPC1 RNAi. In experiments shown on panels A-D the compounds were added 30 minutes prior to the application of glutamate. In experiments shown on panels E-F

neurons were treated at DIV2–4. For each data point the fraction of TUNEL-positive nuclei is shown as mean ± SE (n = 6–8 microscopic fields, 100–300 MSN per field).

Table 1

Perfomance of EVP4593 and its analogs in different assays

EVP cmpnd	HD flies climbing assay (200 μM)	NF-κB inhibition (EC50, nM)	SOC inhibition (Ca^{2+} assay, 0.3 μM)	SOC inhibition (Mn^{2+} assay, 0.3 μM)	SOC inhibition (Ephys assay, 0.3 μM)	*In vitro* HD assay (0.03 – 3.0 μM)
14782	+	7	ND	+	ND	+
4593	+	9	+	+	+	+
14756	+	66	+	+	ND	+
14809	−	1150	ND	ND	ND	+/−
14810	−	1203	ND	−	ND	−
14812	−	8934	ND	−	ND	−
14808	−	> 10000	−	−	−	−

Table 2

Effects of drugs and treatments on glutamate-induced apoptosis in WT and YAC128 MSN

EVP cmpnd (conc)		WT (% TUNEL-positive)				YAC128 (% TUNEL-positive)			
		0μM glutamate		250 μM glutamate		0μM glutamate		250 μM glutamate	
4593	0.03μM	6.75 ± 1.40	(8.98 ± 2.20)	52.37 ± 6.51	(47.07 ± 2.69)	9.12 ± 2.20	(9.09 ± 1.69)	**52.81 ± 3.85***	(81.30 ± 2.76)
	0.3 μM	6.91 ± 1.50	(8.65 ± 1.68)	**20.28 ± 1.22***	(34.84 ± 3.98)	7.88 ± 1.61	(6.55 ± 0.78)	**21.86 ± 2.20***	(71.89 ± 6.05)
	3.0 μM	–		–		–		–	
14756	0.03μM	7.49 ± 2.16	(12.38 ± 2.98)	36.68 ± 4.24	(40.70 ± 5.13)	8.08 ± 1.35	(7.96 ± 1.07)	**48.94 ± 6.97***	(83.99 ± 3.61)
	0.3 μM	6.89 ± 0.75	(7.85 ± 1.19)	31.99 ± 4.33	(39.55 ± 3.49)	6.78 ± 1.93	(8.32 ± 1.28)	**26.70 ± 4.14***	(67.96 ± 5.69)
	3.0 μM	16.43 ± 1.35	(7.85 ± 1.19)	31.62 ± 5.27	(39.55 ± 3.49)	12.13 ± 1.93	(8.32 ± 1.28)	54.71 ± 3.77	(67.96 ± 5.69)
14782	0.03μM	5.59 ± 1.01	(12.38 ± 2.98)	34.84 ± 3.51	(40.70 ± 5.13)	8.40 ± 1.62	(7.96 ± 1.07)	75.09 ± 5.99	(83.99 ± 3.61)
	0.3μM	6.25 ± 2.00	(8.65 ± 1.68)	**17.88 ± 1.50***	(34.84 ± 3.98)	6.01 ± 1.14	(6.55 ± 0.78)	**30.34 ± 3.33***	(71.89 ± 6.05)
	3.0μM	–		–		–		–	
14808	0.03μM	8.76 ± 1.22	(8.98 ± 2.20)	57.43 ± 5.64	(47.07 ± 2.69)	7.10 ± 1.16	(9.09 ± 1.69)	78.33 ± 5.88	(81.30 ± 2.76)
	0.3μM	5.75 ± 1.30	(7.85 ± 1.19)	39.46 ± 4.19	(39.55 ± 3.49)	10.77 ± 2.71	(8.32 ± 1.28)	56.08 ± 4.72	(67.96 ± 5.69)
	3.0μM	5.26 ± 0.83	(6.64 ± 1.32)	37.18 ± 5.04	(39.77 ± 2.56)	5.38 ± 0.84	(5.45 ± 1.07)	75.15 ± 5.35	(81.80 ± 3.84)
14809	0.03μM	14.93 ± 2.00	(12.38 ± 2.98)	42.95 ± 4.63	(40.70 ± 5.13)	9.31 ± 2.49	(7.96 ± 1.07)	70.96 ± 5.21	(83.99 ± 3.61)
	0.3μM	8.76 ± 3.15	(8.65 ± 1.68)	39.39 ± 4.48	(34.84 ± 3.98)	5.97 ± 0.80	(6.55 ± 0.78)	61.37 ± 9.22	(71.89 ± 6.05)
	3.0μM	6.51 ± 1.70	(6.98 ± 0.95)	46.05 ± 2.40	(44.71 ± 4.12)	5.82 ± 1.56	(7.80 ± 1.56)	**53.15 ± 6.42***	(75.75 ± 2.80)
14810	0.03μM	8.31 ± 1.17	(7.59 ± 1.51)	41.95 ± 5.49	(35.29 ± 3.89)	7.72 ± 0.96	(6.97 ± 1.71)	71.98 ± 5.16	(70.24 ± 5.17)
	0.3μM	9.37 ± 1.59	(8.98 ± 2.20)	52.73 ± 4.49	(47.07 ± 2.69)	8.49 ± 2.08	(9.09 ± 1.69)	79.37 ± 3.08	(81.30 ± 2.76)
	3.0μM	5.12 ± 0.62	(7.59 ± 1.51)	33.57 ± 4.88	(35.29 ± 3.89)	6.62 ± 1.06	(6.97 ± 1.71)	64.63 ± 4.41	(70.24 ± 5.17)
14812	0.03μM	5.95 ± 1.59	(7.59 ± 1.51)	40.85 ± 4.61	(35.29 ± 3.89)	6.10 ± 1.16	(6.97 ± 1.71)	68.50 ± 4.62	(70.24 ± 5.17)
	0.3μM	8.97 ± 1.71	(10.67 ± 2.10)	39.16 ± 5.34	(35.90 ± 4.11)	9.15 ± 1.76	(9.28 ± 1.13)	73.68 ± 5.29	(70.27 ± 5.13)
	3.0μM	8.06 ± 1.75	(7.59 ± 1.51)	39.36 ± 3.48	(35.29 ± 3.89)	6.14 ± 0.61	(6.97 ± 1.71)	68.48 ± 6.31	(70.24 ± 5.17)
Ctrl siRNA		19.93 ± 4.24	(12.69 ± 3.19)	40.55 ± 5.35	(36.16 ± 6.51)	26.75 ± 2.77	(19.68 ± 2.34)	60.22 ± 4.19	(63.47 ± 5.87)
TRPC1 siRNA		12.72 ± 2.75	(12.69 ± 3.19)	28.27 ± 5.20	(36.16 ± 6.51)	11.07 ± 2.40	(19.68 ± 2.34)	**36.39 ± 4.24***	(63.47 ± 5.87)

[a] In EVP compound experiment, the number in parenthesis is the untreated control cells in the same batch of MSN culture. In siRNA experiment, the number is the control cells treated with transfection reagent in the same batch of culture.

* P<0.05, compared with control cells and show protective effect.

– toxic, total number of cells are much less than control.